Annals of Nuclear Energy 194 (2023) 110099

Contents lists available at ScienceDirect

Annals of Nuclear Energy

journal homepage: www.elsevier.com/locate/anucene

Review

Multigroup covariance matrix self-shielding effects for thermal reactors fueled with slightly enriched uranium

Adimir dos Santos [a,*], Marcus Vinicius Camilo Galia [a], Luiz Leal [b]

[a] Instituto de Pesquisas Energéticas e Nucleares – IPEN/CNEN-SP, Centro de Engenharia Nuclear (CEN), Av. Prof. Lineu Prestes, 2242, 05508-000 – Cidade Universitária, São Paulo, SP, Brazil
[b] Oak Ridge National Laboratory, PO Box 2008, Oak Ridge, TN 37831, USA

ARTICLE INFO

Keywords:
Multigroup covariance matrix
Indirect Effect
k_{eff} Uncertainty analysis
JENDL 3.3
ERRORR

ABSTRACT

A numerical approach has been successfully developed to treat the self-shielding effects in the multigroup cross section covariance matrices of thermal reactors fueled with slightly enriched uranium. The procedure employs the coupled NJOY/AMPX-II systems developed at IPEN and the ^{238}U resonance parameter covariance data from JENDL 3.3. Only the first two most important ^{238}U resonances are under analyses. The direct and indirect effects of the ^{238}U resonance self-shielding is taken into account. The effect of the change in the cross section is called the direct effect and that of the neutron flux due to change in the cross section is called the indirect effect. The k_{eff} uncertainty analyses applied to the IPEN/MB-01 reveal that the self-shielding effects both direct and indirect have an important bearing on the multigroup covariance matrix as well as on the k_{eff} uncertainty. Also, the indirect effects account for nearly 44% of the total uncertainty. The ERRORR module of the NJOY system is in severe disagreement to the developed method because it considers only the direct effect in the multigroup cross section covariance matrix. Such results underline the application dependence of multi-group cross section covariance matrix, and that ENDF FILE 33 content must be corrected due to the resonance self-shielding effects mainly for applications in thermal reactor fueled with slightly enriched uranium.

1. Introduction

Nuclear data are the results of nuclear physics experiments and evaluated data produced from nuclear models. In any application of nuclear data there is a genuine interest to use the best information that is available and in a convenient form. Among the several types of nuclear data, those describing the neutron-nuclide interactions play an important role in the nuclear science and technology areas. The nuclear reactor applications are their major users.

Nuclear reactor calculations are processes that require a large number of input quantities including those that characterize the neutron-nuclide interactions. The nuclear data represent well-defined physical quantities that have definite but unknown true magnitude. The current knowledge of nuclear data is summarized by its joint probability density function defined so that $f(q_i(E), q_j(E))\Delta q_i, \Delta q_j$ represents the probability that the best-known numerical values of q_i and q_j lies in the range $\Delta q_i \Delta q_j$. Thus, the basic nuclear data are usually known only with a certain margin of certainty and their data accuracy depends on the degree of sophistication with which the measurements and evaluation were performed. Their uncertainties are completely described by their covariance matrix (Peelle, 1982; Smith, 1981; Smith, 1980; Leal et al., 2005).

The nuclear data libraries are organized and released to the general public in the evaluated nuclear data files. Examples of these nuclear data libraries are: ENDF (Brown et al., 2018), JENDL (Shibata et al., 2011) and JEFF (Plompen et al., 2020) among others. These nuclear data libraries by their turn represent the best sources of evaluated nuclear data employing results from experiments available worldwide in conjunction with nuclear data models. Particularly in the resonance region, the SAMMY code (Larson, 2008) plays a major role. This code has been widely used for nuclear data in the resolved and unresolved resonance region. It includes simplified versions of the R-matrix resonance formalism, with the Reich-Moore approach being the most used. One feature of the SAMMY code is the possibility of generating resonance parameter covariance (RPC) as part of the evaluating process.

The nuclear data libraries share an important characteristic. They all have the same format; the ENDF format (Trkov and Brown, 2018). An evaluation for a specific nuclide is subdivided into data blocks called

* Corresponding author.
E-mail addresses: adsantos@alumni.usp.br, asantos@ipen.br (A. dos Santos), niciu86@gmail.com (M. Vinicius Camilo Galia), leallc@ornl.gov (L. Leal).

https://doi.org/10.1016/j.anucene.2023.110099
Received 7 November 2022; Received in revised form 2 July 2023; Accepted 21 August 2023
Available online 30 August 2023

"FILES", identified by the MF-number. The important files for the development of this paper are FILE 2 which provides the data for the resolved resonance parameters and FILE 32 which provides the resolved resonance parameter covariance matrix.

The propagation of the uncertainties of the basic nuclear data to the reactor responses is becoming an essential part of the reactor physics area. The development of the module TSUNAMI of the SCALE system (Wieselquist and Lefebvre, 2023) and the MCNP-WHISPER (Brown et al., 2016) are good examples of codes that deal with this important subject. Particularly, MCNP-WHISPER uses sensitivity profiles and data covariances to select similar benchmarks, determine bias, bias-uncertainty, and margin-of-subcriticality for setting the Upper-Subcritical-Limit. In this context the covariance matrix of the basic nuclear data plays an important role in setting up uncertainty margins in several reactor responses such as the ones related to the criticality safety.

A complete knowledge of the uncertainties in the nuclear reactor responses due to the basic nuclear data is essential for assessing the technical feasibility, safety, and economics of such systems. Furthermore, vital information can be furnished to reactor designers from the results of the estimation of the response uncertainties. They can decide whether or not to improve the basic nuclear data, for example by including integral experiments information. Finally, the nuclear data uncertainty propagation is a requirement for the regulatory bodies in several countries (NRC, 2012).

1.1. A brief overview of the covariance data in the ENDF FILEs

The start points to include the uncertainty data in the ENDF FILEs arose with the advent of ENDF/B-IV (Garber, 1975) in 1975. Still in this decade, an important contribution came in 1979 with the release of ENDF/B-V (Perey, 1977). Besides of introducing an organizational structure for the covariance data, the ENDF/B-V introduced the ENDF FILEs 31, 32, and 33 whose contents presented the covariances, respectively, for the average number of fission neutrons, for the resolved resonance parameters, and for the multigroup cross sections. This library was user-restricted and just a few nuclides was released to the general public. The coming decade (198Ós) showed some advances in the covariance data and also the development of specific routines for the data interpretation (Perey, 1978). Two ENDF/B-V revisions were released with new information and corrections. The ENDF/B-VI (Rose, 1991) was released later on in 1991 followed by several revisions to the covariance FILEs. Very important progresses were made in this decade with the developments of MCNP-WHISPER and the TSUNAMI module of SCALE. JENDL 3.3 (Shibata et al., 2002) was released in 2002. To date, this is the only nuclear data library that released the contents of FILE 32, that is, the covariance matrix for the resolved resonance parameters, to the general public. Of major interests to this work were the covariance matrix for the ^{238}U resolved resonance parameters. Also, in JENDL 3.3 there were resolved resonance covariance data for 26 nuclides. The ENDF/B-VII (Chadwick et al., 2006) was released in 2006 but only FILEs 31 and 33 were released to the general public. This decade witnessed several new methods employing the multigroup cross section covariance (FILE 33) (Vanhanen, 2015; Zwermann et al., 2011) and the utilization of Monte Carlo Methods employing these data in several practical applications. The recently released ENDF/B-VIII (Brown et al., 2018) as its predecessor did not released FILE 32 to the general public; just some improvements in FILE 33. Similarly, JENDL 4.0 (Shibata et al., 2011) did not provide FILE 32 as its predecessor did. In this decade (201Ós) several studies employing uncertainty analyses were performed for basic research and power thermal reactors (Rochman et al., 2017). Some recent works can be found in (Sobes et al., 2021a; Sobes et al., 2021b).

1.2. The resonance self-shielding in the multigroup covariance matrix (FILE 33) and the purpose of this work

The resonance self-shielding is, by definition, the effect of reduction of the neutron flux in the neutron energy region close to the resonance energy of a specific resonance. This phenomenon occurs mainly in the thermal and epithermal energy region, and it is very important for thermal reactors fueled with slightly enriched uranium. In this case, the main nuclide is ^{238}U which exhibits strong resonances in this neutron energy region. Fig. 1 illustrates the self-shielding phenomenon for the IPEN/MB-01 reactor.

Resonance self-shielding also occurs in the construction of FILE 33; the multigroup covariance matrix. The phenomenon of self-shielding in the multigroup covariance matrix appears in the determination of the derivative of the group cross sections to the resonance parameter under consideration. The definition of the group cross section involves two quantities: the cross section and the neutron flux, both as a function on energy. When a perturbation is performed in the resonance parameter both quantities change. The effect of the change in the cross section is called the direct effect and the change in the neutron flux due to change in the cross section is called the indirect effect. Due to that the derivative of the group cross section to the resonance parameter must consider both effects. There are other implications to be taken into account in the resonance self-shielding of the multigroup covariance matrix. These features will be shown in the methodologies developed in this work.

Several methods (Zwermann et al., 2011; Chiba, 2007; Wiarda et al., 2008; Chiba, 2006; Takeda and Foad, 2013; Cullen, 2010; Hiruta et al., 2008), and more recently (Hursin et al., 2020) and (Yu et al., 2018) have been proposed to address this important phenomenon in the multigroup covariance matrix. The first aspect that must be noted in the recent history is that the theme of the multigroup covariance self-shielding phenomenon is a contemporary subject. The second aspect is that all these methods rely on isolated resonances. Neither of these methods consider the phenomenon of resonance mutual shielding. The effect of the neutron flux dip due to the presence of a specific resonance might shield the resonance of other nuclides that have a resonance whose energy is close to the one under consideration and vice-versa. The third aspect and the most important one is that all these methods do not consider the indirect effect due to the neutron flux variation on the derivative of the group cross section with respect to the resonance parameter. These features will become clearer in the method proposed in this paper.

Among the several types of nuclear data involved the portion pertinent to thermal and epithermal energy region the resonance parameter representation of the cross section is of major concern. Particularly in this neutron energy region, the ^{238}U nuclear data play a major role and it is the isotope mostly responsible for the phenomenon of resonance self-shielding. The reactor analyses even nowadays still rely mostly on the multigroup formalism, and an important topic to be dealt in the uncertainty analyses is the resonance self-shielding of the multigroup cross section covariance matrix (FILE 33). This is still an open subject and just few works have addressed this important phenomenon (Boyarinov et al., 2017; Chiba et al., 2014; Leal and de Saint Jean, 2018). This paper aims at contributing to this subject and to present a numerical approach that employs the coupled NJOY/AMPX-II (Dos Santos et al., 2000) system developed at IPEN. The code NJOY version 2016.53 (MacFarlane, 2019) was employed throughout of this paper. With exception to ^{238}U, all other nuclear data come from ENDF/B-VII.0 (Chadwick et al., 2006). The ^{238}U nuclear data are from JENDL 3.3 because this library is the only one available at IAEA-NDS that contains the covariance matrix for the resonance parameters of this nuclide. The JENDL 3.3 resonance parameter covariance matrix (RPC) were generated with the KALMAN code (Kawano and Shibata, 1997).

2. The multigroup covariance matrix and its self-shielding effects

This section describes the propagation of the uncertainties in the basic nuclear data to a generic integral reactor response R. Section 2.1 presents this methodology and its extension to the multigroup

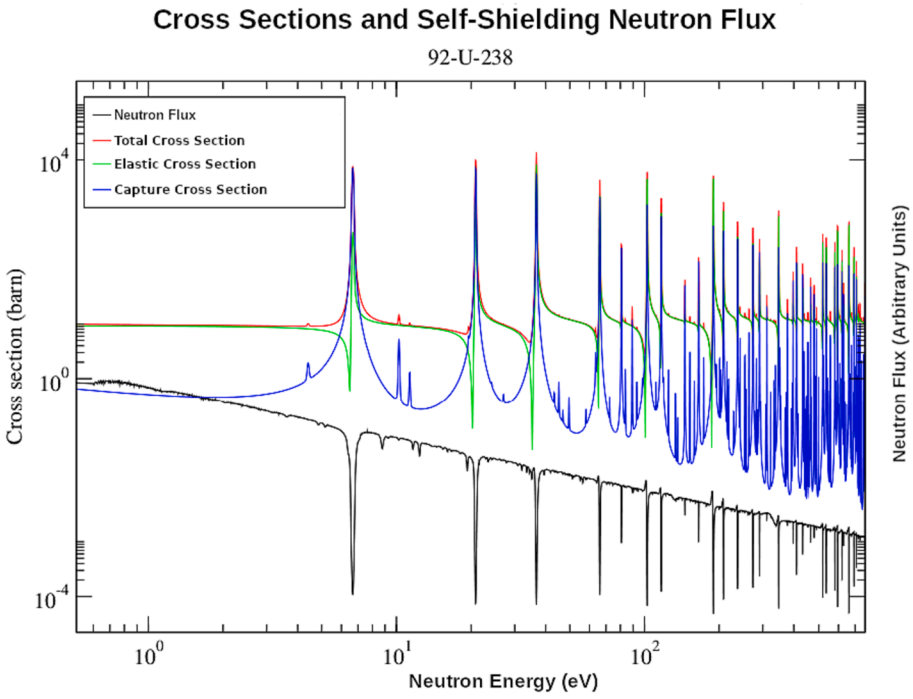

Fig. 1. ^{38}U cross sections and ROLAIDS weighting flux as a function of neutron energy at 293 K.

formalism. Section 2.2 presents the extension of the multigroup covariance formalism to the thermal and epithermal energy region.

2.1. Uncertainty of the reactor response r due to the nuclear data uncertainties

The variance of the reactor response R due to the uncertainties in the basic nuclear data is given by: (Dos Santos, 1984):

$$\frac{V(R)}{R_0^2} = \int\int\int\int S(\vec{r},E)Q(E,E')S^T(\vec{r}',E')dVdV'dEdE' \tag{1}$$

where steady state and no angular dependence were for simplicity considered, $S(\vec{r},E)$ is defined as the sensitivity vector, $S^T(\vec{r}',E')$ is its transpose, and $Q(E,E')$ is the relative covariance matrix (Perey, 1977) whose elements are:

$$Q_{i,j}(E,E') = \frac{cov\left(p_i(E),\, p_j(E')\right)}{p_i(E) \bullet p_j(E')}; \tag{2}$$

In Eq. (2) p_i and p_j are two generic nuclear data, respectively at energy E and E' and $cov\left(p_i(E),p_j(E')\right)$ is its covariance. $S_i\left(r,E\right)$ is a vector whose components to a generic nuclear data p_i are given by:

$$S_i\left(r,E\right) = \frac{p_i}{R(t)}\frac{dR}{dp_i} \tag{3}$$

with

$$\frac{dR}{dp_i} = \frac{\partial R}{\partial p_i} + \frac{\partial R}{\partial \phi} \bullet \frac{d\phi}{dp_i} \tag{4}$$

where the first term of Eq. (4) is the direct effect of the nuclear data on the integral response R while the second one is the indirect effect.

Practical applications of uncertainty analysis adopt the multigroup formalism (Vanhanen, 2015) which requires the use of group cross section sensitivities and their corresponding correlation matrices. In this case the uncertainty analysis is made in two parts. In the first part, the uncertainty in the basic nuclear data field is propagated to the group cross sections and in the second part these uncertainties are propagated to the reactor responses. Let the nuclear reactor response $R(t)$ be an explicit functional of some specific components of the microscopic group cross section vector σ defined as follow:

$$\sigma = \left[\sigma_{11}^1, \sigma_{12}^1, \cdots, \sigma_{1G}^1, \sigma_{11}^2, \cdots, \sigma_{1g}^j, \cdots, \sigma_{lg}^j, \ldots, \sigma_{MG}^{JJ}\right] \tag{5}$$

where σ_{lg}^j denotes the microscopic group cross section of nuclide l, group g, nuclear reaction type j, M is the total number of nuclides, G is the number of groups, and JJ is the number of types of nuclear data considered. The sensitivity coefficient vector, $\underset{\sim}{S}\left(\underset{\sim}{r},E\right)$ given by Eq. (3) can be split into two parts as:

$$S\left(r,E\right) = SR\sigma(r) \bullet S\sigma p(r,E) \tag{6}$$

where $SR\sigma(r)$ is defined as the microscopic group cross section sensitivity vector and it is given by:

$$SR\sigma(r) = \left[\frac{\sigma_{11}^1}{R} \bullet \frac{dR}{d\sigma_{11}^1}, \frac{\sigma_{12}^1}{R} \bullet \frac{dR}{d\sigma_{12}^1}, \ldots, \frac{\sigma_{lg}^j}{R} \bullet \frac{dR}{d\sigma_{lg}^j}, \ldots, \frac{\sigma_{MG}^{JJ}}{R} \bullet \frac{dR}{d\sigma_{MG}^{JJ}}\right] \tag{7}$$

and $S\sigma p(r,E)$ is a matrix defined as:

$$\underset{\sim}{S}\underset{\sim}{\sigma p}\left(\underset{\sim}{r},E\right) = \begin{bmatrix} \frac{p_1}{\sigma_1^{11}}\frac{d\sigma_{11}^1}{dp_1} & \cdots & \frac{p_j}{\sigma_1^{11}}\frac{d\sigma_{11}^1}{dp_j} & \cdots & \frac{p_{JJ}}{\sigma_{11}^1}\frac{d\sigma_{11}^1}{dp_{JJ}} \\ \vdots & \ddots & & & \vdots \\ \frac{p_1}{\sigma_{ig}^j}\frac{d\sigma_{ig}^j}{dp_1} & \cdots & \frac{p_j}{\sigma_{lg}^j}\frac{d\sigma_{lg}^j}{dp_j} & \cdots & \frac{p_{JJ}}{\sigma_{ig}^j}\frac{d\sigma_{ig}^j}{dp_{JJ}} \\ & \vdots & & \ddots & \vdots \\ \frac{p_1}{\sigma_{MG}^{JJ}}\frac{d\sigma_{MG}^{JJ}}{dp_1} & \cdots & & \frac{p_{JJ}}{\sigma_{MG}^{JJ}}\frac{d\sigma_{MG}^{JJ}}{dp_{JJ}} & \end{bmatrix} \tag{8}$$

Eq. (1), the quadratic form of the uncertainty of the response $R(t)$,

can be written in terms of $S\,R\sigma\left(\underset{\sim}{r}\right)$ and $S\,\sigma p(r,E)$, given respectively by Eqs. (7) and (8), as:

$$\left(\frac{\sigma_R}{R}\right)^2 = \int dV \int dV' \underset{\sim}{S}\,R\sigma\left(\underset{\sim}{r}\right)\underset{\sim}{\Theta}\left(\underset{\sim}{r},\underset{\sim}{r}',\underset{\sim}{\sigma}\right)\underset{\sim R\sigma}{S^T}(\vec{r}') \tag{9}$$

where the matrix $\underset{\sim}{\Theta}\left(\underset{\sim}{r},\underset{\sim}{r}',\underset{\sim}{\sigma}\right)$ is given by:

$$\underset{\sim}{\Theta}\left(\underset{\sim}{r},\underset{\sim}{r}',\underset{\sim}{\sigma}\right) = \int^d E \int^d E' \underset{\sim\sim}{S}\,\sigma p\left(\underset{\sim}{r},E\right)\underset{\sim}{Q}(E,E')\underset{\sim\sigma p}{S^T}\left(\underset{\sim}{r}',E'\right) \tag{10}$$

and it is a square matrix whose elements are given by:

$$\Theta^{kl}_{gg'}\left(\underset{\sim}{r},\underset{\sim}{r}',\underset{\sim}{\sigma}\right) = \sum_m\sum_n \int^d E \int^d E' S^{km}_{\sigma g}\left(\underset{\sim}{r},E\right) Q_{mn}(E,E') S^{Tnl}_{\sigma g'}\left(\underset{\sim}{r}',E'\right) \tag{11}$$

$\underset{\sim}{\Theta}\left(\underset{\sim}{r},\underset{\sim}{r}',\underset{\sim}{\sigma}\right)$ represents the covariance matrix of the group cross section (σ^j_{lg}). The superscript kl in Eq. (11) refers, respectively, to nuclear reaction k and nuclide l. $S^{ij}_{\sigma g}(\vec{r},E)$ represents the elements of the matrix $S\,\sigma p(r,E)$ given in Eq. (8). The superscript ij in $S^{ij}_{\sigma g}(\vec{r},E)$ refers to either the superscripts km or to nl both in Eq. (11). The sums $\Sigma_m\Sigma_n$ extend for all correlations among pieces of nuclear data of all nuclides present in the uncertainty analyses.

The elements of the matrix $\Theta^{kl}_{gg'}\left(\underset{\sim}{r},\underset{\sim}{r}',\underset{\sim}{\sigma}\right)$ represent the covariance of the group cross section for all possible neutron-nucleus interactions and for all nuclides presents in the analyses. It must be noted that $\Theta^{kl}_{gg'}(\vec{r},\vec{r}',\sigma)$ is reactor region dependent and the correlation among these regions is also taken into consideration. Thus, the two-phase procedure to extend the uncertainty analyses to the group formalism is completely established.

2.2. Extension of the multigroup covariance formalism to the thermal and epithermal energy region

The resolved resonance parameters for the actinide nuclides constitute one source of uncertainty in thermal reactor calculations. They are given in the ENDF FILE 2 under MT reaction number 151. The number of resolved resonances has increased significantly in the recent nuclear data libraries and the treatment of the effect of their uncertainties to the reactor responses is a major challenge in the field of reactor physics. In order to extend the uncertainty analysis in the multigroup formalism given by Eqs. (9) through (11) for thermal and epithermal energy region consider, for simplicity, just one single actinide nuclide and an infinite medium. Then, $Q_{i,j}$ given by Eq. (2) will depend only on the resolved resonance parameters and their corresponding covariance matrix for the actinide nuclide under consideration. Furthermore, the dependence of $Q_{i,j}$ on E, and E' is taken in a discrete way for the same or different resonances as $Q_{i,j}(E_{0i},E'_{0j})$. Here, E_{0i} and E'_{0j} represent, respectively, the resonance energies for the resonances i in group g, and for the resonances j in group g'. The groups g and g' might contain a single, a set or parts of resonances. Consequently, the integrals involving E, and E' in Eq. (11) are taking into consideration as a sum for all possible resonance contributions in groups g and g'. Considering all these simplifications Eq. (19) can be rewritten in a convenient form and in a consistent way to the formalism given in Leal and de Saint Jean (2018) as:

$$\Theta^k_{g,g'} = \sum_i\sum_j \frac{d\sigma^k_g}{dp_i} cov\,(p_i,\,p_j)\,\frac{d\sigma^k_{g'}}{dp_j} \tag{12}$$

where the subscript l in σ^k_g and $\sigma^k_{g'}$ has been dropped since there is only one nuclide under consideration, the spatial dependence was omitted for simplicity, $\Theta^{kl}_{g,g'}(\vec{r},\vec{r}',\sigma)$ was replaced by $\Theta^k_{g,g'}$ and the superscript k represents the nuclear reaction under consideration in the resolved neutron energy region (total, elastic, (n,γ) or (n,f)). $\Theta^k_{gg'}$ is referred as the elements of the multigroup cross section covariance matrix and is given in FILE 33 of ENDF and $cov\left(p_j,p_j\right)$ is the resonance parameter covariance matrix given in FILE 32 of ENDF.

Since $cov\left(p_j,p_j\right)$ is a basic nuclear data set known a priori and provided in FILE 32 of ENDF, the question to determine the elements of the multigroup cross section covariance matrix ($\Theta^k_{g,g'}$) reduces to the one of determining the derivatives of the group cross section (σ^{kg}) with respect to the resonance parameter (p_i) and (p_j).

The group cross section σ^k_g follows its standard definition (Bell and Glasstone, 1979) and is given by:

$$\sigma^k_g = \frac{\int_{E_g}^{E_{g+1}} \sigma^k(E)\Phi(E)dE}{\phi_g}, \tag{13}$$

where $\sigma^k(E)$ and $\Phi(E)$ are, respectively the energy dependents, microscopic cross section for the nuclear reaction k and the neutron flux or spectrum in the reactor region under consideration, E_g and E_{g+1} represent, respectively, the lower and upper neutron energy bounds of group g, and ϕ_g is the neutron flux group defined as:

$$\phi_g = \int_{E_g}^{E_{g+1}} \Phi(E)dE \tag{14}$$

The derivative $\frac{d\sigma^{kg}}{dp_l}$; l equal to either i or j in Eq. (12), can immediately be found from Eq. (13) as:

$$\frac{d\sigma^k_g}{dp_l} = \underbrace{\frac{1}{\Phi_g}\int\left(\frac{\partial\sigma^k(E)}{\partial p_l}\right)\Phi(E)dE}_{Direct\ \ Effect} + \underbrace{\frac{1}{\Phi_g}\int\sigma^k(E)\left(\frac{\partial\Phi(E)}{\partial p_l}\right)dE - \frac{\sigma^{kg}\int\left(\frac{\partial\Phi(E)}{\partial p_l}\right)dE}{\Phi_g}}_{Indirect\ \ Effect} \tag{15}$$

Similarly, to sensitivity analysis problems, the first term of Eq. (15) can be interpreted as the direct effect of the nuclear data p_l on $\frac{d\sigma^k_g}{dq_l}$. The second and third terms of this equation are the indirect effect, i.e., the effect of the neutron flux $\Phi(E)$ on $\frac{d\sigma^k_g}{dq_l}$. The direct effect is easier to found because in the thermal and epithermal energy region $\sigma^k(E)$ is an explicit function of p_l. Contrary to that $\Phi(E)$ is an implicit function of p_l since the effect of its uncertainty is propagated to the cross section $\sigma^k(E)$ which by its turn is propagated to $\Phi(E)$ through the solution of the neutron transport equation which depends on $\sigma^k(E)$. Eqs. (12) through (15) are the basic equations to obtain the multigroup cross section covariance matrix.

The great difficult to apply Eq. (15) in thermal reactors fueled with slightly enriched uranium is the determination of $\Phi(E)$ and consequently its derivative $\frac{\partial\Phi(E)}{\partial p_l}$. The neutron flux or spectra ($\Phi(E)$) is strongly application dependent and might impose severe restriction on the determination of $\frac{d\sigma^k_g}{dp_l}$.

3. The multigroup covariance methodologies applied to the IPEN/MB-01 reactor

The following developments consider the methodologies for the determination of the multigroup covariance matrix only for ^{238}U since this actinide nuclide is the main contributor to the resonance self-shielding phenomenon in the epithermal neutron energy region of light water reactors fueled with slightly enriched uranium. This nuclide possesses a huge amount of resolved resonances and due to that the analyses will be restricted to the neutron energy groups that contains its

most important resonances. The methodologies employed to analyze the effects of the self-shielding in the multigroup covariance matrices shown in Fig. 2 were based in the coupled systems NJOY/AMPX-II (Dos Santos et al., 2000) developed at the Nuclear Engineering Center of IPEN/CNEN-SP. An epithermal neutron group energy structure of 54 groups (Barhen et al., 1978) is employed throughout of the analyses. However, only groups (11) and (15) of the NJOY 54 multigroup structure will be under consideration here. Group (11) spans the neutron energy interval from 6.4763 eV to 8.3012 eV while group (15) from 17.60 eV to 22.60 eV. Groups (11) and (15) contain, respectively, the most important ^{238}U s-wave resonances located at 6.67 eV and 20.871 eV. The applications of all methodologies to obtain the multigroup covariance matrix developed in this work will be applied to the IPEN/MB-01 research reactor facility. This reactor is a thermal critical facility which consists of a 28×26 array of UO_2 fuel rods, 4.3% enriched and clad by stainless steel (type 304) inside of a light water tank. The IPEN/MB-01 reactor has been part of several benchmark activities in the NEA/OECD projects IRPhE (International Reactor Physics Experiments) and ICSBEP (International Criticality Safety Benchmark Evaluation Project.). A more detailed description of the IPEN/MB-01 reactor can be found in references (Dos Santos et al., 2004; Dos Santos et al., 2005).

The calculation methodologies to obtain the multigroup covariance matrices shown in Fig. 2 exploits the capabilities of the NJOY system to get the linearized cross sections employing the Reich-Moore formalism (Arbanas et al., 2017) and to perform the cross-section Doppler Broadening at specific temperatures. The ROLAIDS module of AMPX-II (Green et al., 1976) is an epithermal cell code and employs a collision probability method in conjunction with pointwise cross sections from NJOY. It takes into account both space and energy self (and also mutual) shielding to get the neutron flux ($\Phi(E)$). As will be shown the neutron flux from ROLAIDS will be of major importance to get the derivative $\frac{\partial \Phi(E)}{\partial p_l}$ and consequently the indirect effects on the determination of derivatives $\frac{d\sigma_g^k}{dp_l}$ given by Eq. (15).

All ROLAIDS runs employed the unit cell of the core of the IPEN/MB-01 reactor as shown in Fig. 3. The IPEN/MB-01 unit cell is composed of a fuel region containing UO_2, a homogenized region composed of the fuel cladding (SS-304) and gap, and a third region filled with light water. The fuel region was further divided into 10 concentric equal area zones to get the resonance self-shielding effects inside of the fuel pellet. The ROLAIDS model is comprised of twelve zones which are numbered starting from the cylindrical cell center. Zones 1 through 10 refers to the UO_2 region and R_1 through R_{10} as shown Fig. 3 are their corresponding radius. Zones 11 and 12 correspond, respectively to the homogenized clad and the light water moderator. This unit cell employs the Wigner-Seitz approximation (Bell and Glasstone, 1979) and was run in the equivalent cylindrical geometric shown in Fig. 3 with white boundary condition at the outermost zone. The neutron flux $\Phi(E)$ and the average group cross sections in the epithermal neutron energy region are calculated for each one of the twelve IPEN/MB-01 zones.

Four distinct methodologies were developed to obtain the multi-

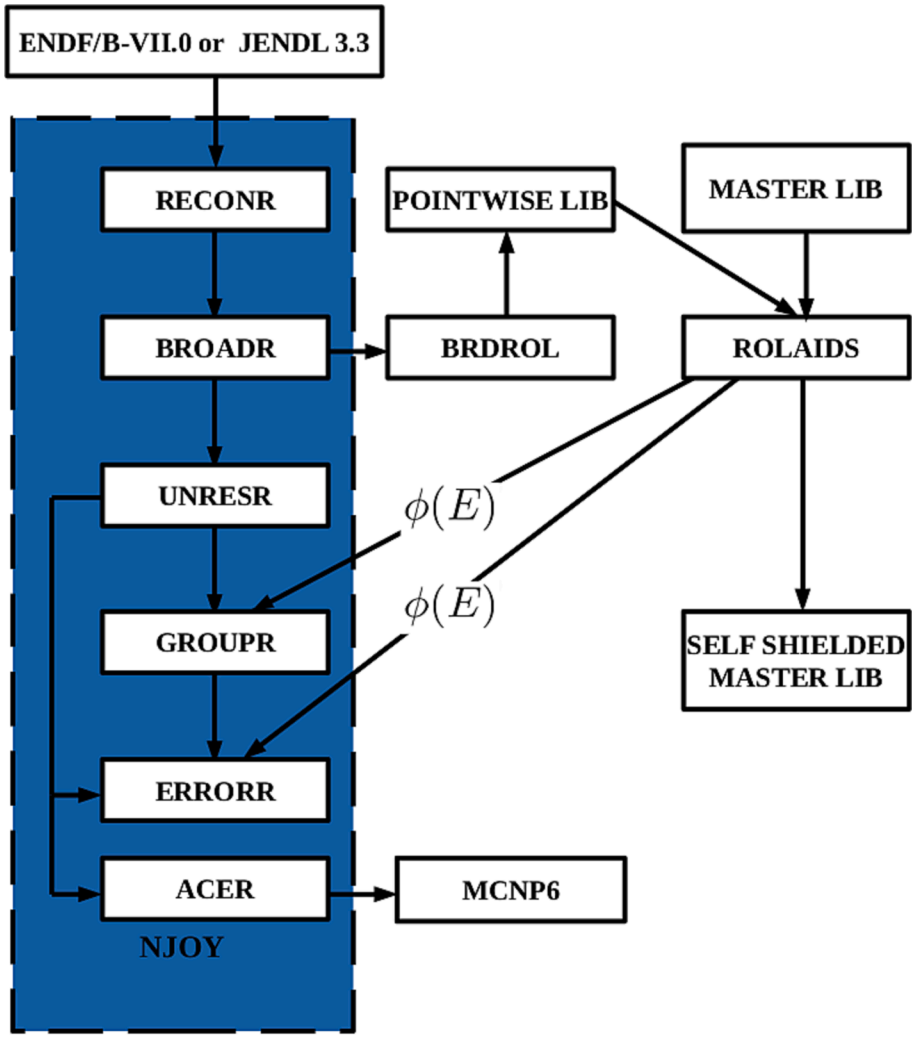

Fig. 2. The calculation methodology flowchart.

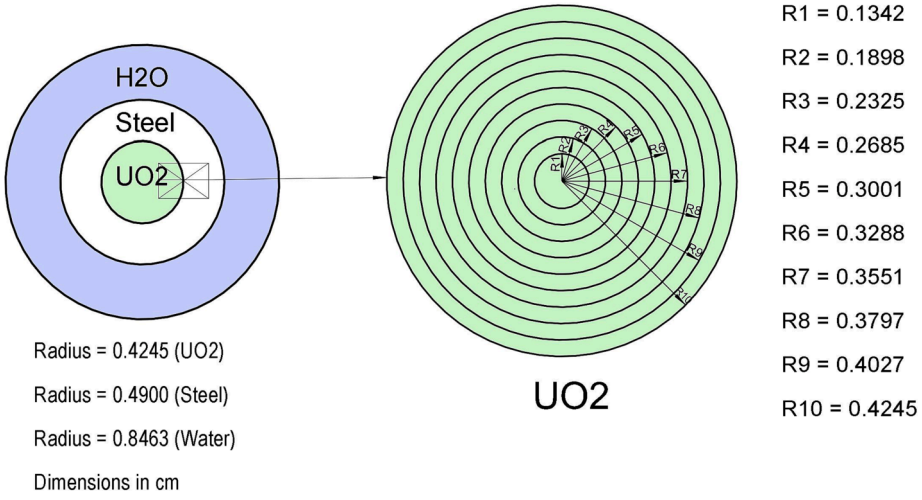

Fig. 3. Unit cell of the IPEN/MB-01 reactor.

group cross section covariance matrices for ^{238}U employing the flowchart shown in Fig. 2. These methodologies will be applied to the IPEN/MB-01 reactor. The first three methodologies can be applied to any one of the 10 zones of the IPEN/MB-01 unit cell shown in Fig. 3. The index i specifying the zone number was omitted for simplicity. This is a practical application, and it will show the difficulties to get the multigroup covariance matrices in a real situation. All methodologies use the covariance matrix from FILE 32 of JENDL3.3. This library provides covariance data for the parameters of twenty-six ^{238}U resolved resonances.

The first methodology employs the NJOY built-in approach to calculate the multigroup covariance matrices. The RECONR, BROADR, and UNRESR modules are used to reconstruct, to Doppler broaden the ^{238}U cross sections, and to calculate the self-shielding effects in the unresolved resonance region, respectively. The pointwise cross sections produced by BROADR are transferred to the ROLAIDS module of AMPX-II by the in-house interface module BRDROL (Dos Santos et al., 2000). The self-shielding treatment of the actinide resolved resonances in the neutron energy region from 0.625 eV to 5.53 keV is carried out by ROLAIDS thanks to the unit cell of the IPEN/MB-01 reactor shown in Fig. 3. The neutron flux ($\Phi(E)$) as a function of the neutron energy and for a specific zone of the unit cell is used by the NJOY modules GROUPR and ERRORR as a weighting function. These NJOY modules transform pointwise cross section from UNRESR and the JENDL 3.3 FILE 32 into multigroup cross sections and multigroup cross section covariance matrices.

The second methodology considers Eq. (12) and the derivative $\frac{d\sigma_g^k}{dp_i}$ calculated directly from Eq. (15). A numerical approach was adopted to get the derivatives $\frac{\partial\sigma^k(E)}{\partial p_i}$ and $\frac{\partial\Phi(E)}{\partial p_i}$ considering two perturbed cases: The ^{238}U resonance parameters in groups (11) and (15) are individually perturbed (one group and one resonance parameter each time) by a small amount ($+\sigma$ and $-\sigma$ values). These perturbed ^{238}U libraries were employed individually (one perturbation each time) for the subsequent NJOY and ROLAIDS runs. The derivatives $\frac{\partial\sigma^k(E)}{\partial p_i}$ and $\frac{\partial\Phi(E)}{\partial p_i}$ are calculated numerically as:

$$\frac{\partial\sigma^k(E)}{\partial p_i} = \frac{\Delta\sigma^k(E)}{2\bullet(\Delta p_i)} = \frac{\sigma^{k+}(E)-\sigma^{k-}(E)}{2\bullet(p_i^+ - p_i^-)} \tag{16}$$

and

$$\frac{\partial\Phi(E)}{\partial p_i} = \frac{\Delta\Phi(E)}{2\bullet(\Delta p_i)} = \frac{\Phi^+(E)-\Phi^-(E)}{2\bullet(p_i^+ - p_i^-)} \tag{17}$$

where the superscript $+$ and $-$ represents, respectively, the ($+\sigma$ and $-\sigma$) values of the quantity under consideration in Eq:s (16) and (17).

Some other auxiliary programs were written to discretize $\sigma^k(E)$, $\frac{\partial\sigma^k(E)}{\partial p_i}$, and $\frac{\partial\Phi(E)}{\partial p_i}$ in the same energy grid and to perform the integrals of Eq. (15) employing the Simpson's rule (Velleman, 2005). The derivatives $\frac{d\sigma_g^k}{dp_i}$ were calculated for the capture, scattering and total cross sections for groups (11) and (15), and for the resonance parameters Γ_n (neutron width) and Γ_γ (capture width). The direct and the indirect effects on the determination of $\frac{d\sigma_g^k}{dp_i}$ implicit in Eq. (15) are taking into consideration in a straightforward fashion.

The third methodology considers Eq. (12) and the perturbed group cross sections given by Eq. (13) from the ROLAIDS output. The derivative $\frac{d\sigma_g^k}{dp_i}$ as in the second methodology is calculated numerically considering two perturbed cases for the resonance parameters. The net results after this sequence of calculations are perturbed values for the ^{238}U group cross sections (σ_g^k) from ROLAIDS. $\frac{d\sigma_g^k}{dp_i}$ is calculated numerically as:

$$\frac{d\sigma_g^k}{dp_i} = \frac{\Delta\sigma_g^k}{2\bullet(\Delta p_i)} = \frac{\sigma_g^{k+}-\sigma_g^{k-}}{2\bullet(p_i^+ - p_i^-)} \tag{18}$$

where the superscripts $+$ and $-$ have the same meaning as before. This derivative is calculated for the capture, scattering and total cross sections for groups (11) and (15), and for the resonance parameters Γ_n and Γ_γ. This numerical procedure to calculate $\frac{d\sigma_g^k}{dp_i}$ already considers the direct and indirect effects since when the resonance parameter is altered, it directly changes the cross section $\sigma^k(E)$ and the neutron flux $\Phi(E)$ needed in Eq. (13). It changes $\sigma^k(E)$ because this quantity is an explicit function of the resonance parameters, and it changes the neutron flux ($\Phi(E)$) because this quantity is the result of the solution of the integral transport equation that depends on $\sigma^k(E)$.

The fourth methodology considers the utilization of the MCNP6 code (Werner et al., 2018) and the ACER module of the NJOY system as shown in Fig. 2. This NJOY module was employed to build the ^{238}U library from JENDL 3.3 for MCNP6. The remainder nuclides needed for the MCNP6 runs arose from its built-in library based on ENDF/B-VII.0 (the isotopes in the ACER library have the suffix.70c). The temperature considered was 293 K for all MCNP6 cases. The purpose of the fourth methodology is to provide independent and very accurate results to verify the validity of the derivative of the cross sections to the resonance parameters and the multigroup covariance matrices provided by the 2nd and 3rd methodologies. The MCNP6 model considers the 3-D benchmark model (Dos Santos et al., 2018) and models explicitly the

fuel rods and their internal parts (UO_2, cladding and gap, alumina region, and spacer tube), guide tubes as well as the control rods, the lower grid plate, the moderator and the radial and axial reflectors composed of light water. The control rods were all aligned and positioned to the measured axial critical position. Tallies were requested for the ^{238}U capture and elastic reaction rates and for the neutron flux for the entire fuel region and for the neutron energy intervals corresponding to groups11and 15. These tallies were calculated for the whole IPEN/MB-01 core. The average group cross sections (capture and elastic) for groups 11 or 15 were obtained accordingly as:

$$\sigma_g^k = \frac{ReactionRateTallyforreactionkandgroupg}{NeutronFluxTallyforgroupg} \bullet \frac{1}{238UNumberDensity} \quad (19)$$

MCNP6 runs considered the ($+\sigma$ and $-\sigma$) perturbations values in the ^{238}U resonance parameters as before and the derivatives $\frac{d\sigma^{kg}}{dp_i}$ were found as:

$$\frac{d\sigma_g^k}{dp_i} = \frac{(\sigma_g^{k+} - \sigma_g^{k-})}{2 \bullet \Delta p_l} \quad (20)$$

where now σ_g^{k+} and σ_g^{k-} are from Eq. (19).

The MCNP group average cross section given by Eq. (19) and consequently the derivatives $\frac{d\sigma^{kg}}{dp_i}$ given by Eq. (20) are averaged for the whole fuel region. The third methodology (ROLAIDS) were compatibilized to that of MCNP6 by calculating its average ^{238}U cross sections for the entire fuel pellet region and for each group as:

$$\overline{\sigma}_g^k = \frac{\sum_{i=1}^{10} (\sigma_g^k)_i \bullet \Phi_{ig} \bullet V_i}{\sum_{i=1}^{10} \Phi_{ig} \bullet V_i} \quad (21)$$

where $\overline{\sigma}_g^k$ is the average ^{238}U cross sections for the entire fuel pellet (zones 1 through 10), k represents the ^{238}U reaction rate, g is the neutron group, $(\sigma_g^k)_i$, $\bullet\Phi_{ig}$, and V_i are, respectively, the ^{238}U group cross section, the neutron group flux, and the volume, all for pellet zone i. Subsequently the cross sections $\overline{\sigma}_g^k$ calculated for the ($+\sigma$ and $-\sigma$) perturbations are replaced in Eq. (20) to get the ROLAIDS estimate of $\frac{d\sigma_g^k}{dp_i}$.

4. Numerical results applied to the IPEN/MB-01 reactor

This section has five purposes. First to report the values of the derivatives of the ^{238}U capture and elastic cross sections to the resonance parameters Γ_γ and Γ_n and the ^{238}U multigroup covariance matrices for the same neutron reactions. Second to present the self-shielding factor for these derivatives and for the multigroup covariance matrices. Third to compare the NJOY covariance matrix to those of the 2nd methodology. Fourth, to compare these quantities derived by the developed methodologies to those derived by MCNP6. Fifth, to perform the k_{eff} uncertainty analyses of a critical configuration of the IPEN/MB-01 reactor. The analyses are performed in the neutron energy groups that incorporate the most two important low-lying ^{238}U resonances and located respectively at 6.67 and 20.8710 eV. Fig. 1 shows these resonances. The reason of the choice of these two ^{238}U resonances is their crucial importance for the determination of the IPEN/MB-01 k_{eff} and its uncertainty. As mentioned previously in Section 3, group (11) spans the neutron energy interval from 6.4763 eV to 8.3012 eV while group (15) from 17.60 eV to 22.60 eV. Group (11) incorporates the first ^{238}U resonance while group (15) the second one. The precisions employed by NJOY to reconstruct and to Doppler Broaden the ^{238}U cross section were 10^{-3} for 0 K and 293 K, 10^{-4} for 600 K and 900 K, and $5x10^{-5}$ for 1200 K. The precision employed by ROLAIDS to get the neutron flux and consequently the group average cross sections was 10^{-5} for all cases. The symbols DGN and DGG employed in this section represent that the derivatives in consideration were taken respectively to Γ_n and Γ_γ.

All the numerical results from Sections 4.1 through 4.4.2 refer to the UO_2 innermost zone (zone number 1) of the IPEN/MB-01 unit cell as shown in Fig. 3. This innermost zone has the strongest ^{238}U resonance self-shielding effects.

The MCNP6 models a 3-D model of the IPEN/MB-01 reactor and its cross section derivatives and multigroup covariance matrices refer to the whole UO_2 fuel rods in the core. Equations (20) and (21) of Section 3.0 are employed to make the results of the 3rd methodology compatible to those of MCNP6. This comparison is shown in Section 4.4.3 and Section 4.5 shows the IPEN/MB-01 k_{eff} uncertainty analyses.

The criterion for the choice of the size of the perturbation in the resonance parameters was the agreement between the calculated values of the derivatives of the group cross section $\frac{d\sigma^{kg}}{dp_i}$ arising from the 2nd and 3rd methodologies. The goal was to find an agreement lower than 1% for all derivatives. As shown in Table 1, this goal was attended for a perturbation of 0.0625% in the resonance parameters and it was applied to 2nd and 3rd methodologies to get the derivative $\frac{d\sigma^{kg}}{dp_i}$.

The resonance parameter covariance data of interest to this work extracted from FILE 32 of JENDL 3.3 are shown in Table 2. The only coupling allowed is from the first resonance to the second one and vice-versa. This simplified model allows the application of the developed methodologies because it considers just the two aforementioned ^{238}U resonances, the interpretation of each term of the multigroup covariance matrix given by Eq. (12), and the intercomparison of all methodologies developed in this work. The data of Table 2 are absolute values, and the nominal values for the resonance parameters are given in Table 3. JENDL 3.3 does not report any uncertainty to the resonance energy E_0 and this resonance parameter was kept in Table 1 just for consistency to its FILE 32. Table 2 is a symmetric square matrix whose diagonal elements represent the variance of the resonance parameters. The diagonal elements are necessarily positive because their square root represent the uncertainty of the corresponding resonance parameters given in Table 3. Furthermore, Table 2 shows that there are correlations between Γ_n and Γ_γ in the same group and between groups (11) and (15). The covariance between Γ_n and Γ_γ in group (11) is positive and consequently these parameters are classified as correlated. The same does not occur for group (15) since the covariance between Γ_n and Γ_γ is negative and consequently they are anti-correlated. The covariance between groups shows that Γ_n is correlated and Γ_γ is anti-correlated. Finally, Γ_n from group (11) and Γ_γ from group (15) are anti-correlated and conversely, they are correlated. These aspects will be important for the interpretations of the results of the multigroup covariance matrix.

4.1. The determination of the derivatives $\frac{\partial\sigma^k(E)}{\partial p_i}$ and $\frac{\partial\Phi(E)}{\partial p_i}$

The derivatives $\frac{\partial\sigma^k(E)}{\partial p_i}$ and $\frac{\partial\Phi(E)}{\partial p_i}$ were determined according to the numerical approach described for the 2nd methodology in Section 3.0. Eqs. (16) and (17) in conjunction with the flowchart shown in Fig. 2

Table 1
Relative difference between 2nd and 3rd methodologies (%).

	1-σ perturbation values			
	1%	0.5%	0.25%	0.0625%
$\frac{d\sigma_{11}^{\gamma}}{d\Gamma_\gamma}$	−14.53	−28.16	1.71	−3.20E-02
$\frac{d\sigma_{11}^{s}}{d\Gamma_\gamma}$	−4.53	−8.01	−0.58	0.00E + 00
$\frac{d\sigma_{11}^{t}}{d\Gamma_\gamma}$	−9.71	−18.57	0.60	−1.63E-02
$\frac{d\sigma_{11}^{\gamma}}{d\Gamma_n}$	−0.939	−2.75	2.26	1.32E-01
$\frac{d\sigma_{11}^{s}}{d\Gamma_n}$	−2.834	−7.29	−2.80	−1.24E-01
$\frac{d\sigma_{11}^{t}}{d\Gamma_n}$	−1.647	−1.90	3.09	1.51E-01

Table 2
Resonance parameter covariance matrix for the first and second ^{238}U resonance. (eV^2).

	Group (11)			Group (15)		
	First Resonance Resonance Energy (E_0)	Neutron Width (Γ_n)	Gamma Width (Γ_γ)	Second Resonance Resonance Energy (E_0)	Neutron Width (Γ_n)	Gamma Width (Γ_γ)
E_0	0.00000E + 00	0.00000E + 00	0.00000E + 00	0.00000E + 00	0.00000E + 00	0.00000E + 00
Γ_n		9.21014E-10	1.68979E-08	0.00000E + 00	1.58580E-08	−5.04550E-08
Γ_γ			3.10649E-07	0.00000E + 00	2.88346E-07	−9.11603E-07
E_0				0.00000E + 00	0.00000E + 00	0.00000E + 00
Γ_n					2.99375E-06	−7.39363E-06
Γ_γ						2.01901E-05

Table 3
Resonance parameters for the first and second ^{238}U resonance (eV).

First Resonance			Second Resonance		
Resonance Energy $(E_0)_0$	Neutron Width (Γ_n)	Gamma Width (Γ_γ)	Resonance Energy (E_0)	Neutron Width (Γ_n)	Gamma Width (Γ_γ)
6.67000E + 00	1.49000E-03	2.30000E-02	2.08710E + 01	1.02600E-02	2.29100E-02

were extensively employed to obtain these derivatives. Initially, it has been found that the derivative $\frac{\partial\sigma^k(E)}{\partial p_l}$ independently of the neutron reaction and resonance parameter considered has a symmetric shape centered in the resonance energy E_0. Fig. 4 shows representative results for the derivative of the ^{238}U (n,γ) cross section at 293 K and 600 K for the resonances located at 6.67 eV (Fig. 4(a)) and at 20.871 eV (Fig. 4 (b)). Several details can be noted in this figure. The derivative shapes are not necessarily equal to that of the corresponding cross sections. $\frac{\partial\sigma(n,\gamma)}{\partial\Gamma_n}$ for both resonances and $\frac{\partial\sigma(n,\gamma)}{\partial\Gamma_\gamma}$ for the resonance located at 20.871 eV are always positive and have similar shapes to the corresponding cross section in their whole neutron energy domains. However, the same does not occur for $\frac{\partial\sigma(n,\gamma)}{\partial\Gamma_\gamma}$ for the resonance located at 6.67 eV shown in Fig. 4 (a). This derivative shows a shape completely different from that of the $\sigma(n,\gamma)$ cross section. It shows alternate signs (positive and negative) depending on the neutron energy intervals, and it has two additional small peaks and a pronounced dip.

The Doppler Broadening of the derivatives $\frac{\partial\sigma(n,\gamma)}{\partial\Gamma_n}$ and $\frac{\partial\sigma(n,\gamma)}{\partial\Gamma_\gamma}$ shown in Fig. 4 has the same characteristics of the corresponding cross sections. The resonance width increases for both derivatives. The resonance peak decreases for $\frac{\partial\sigma(n,\gamma)}{\partial\Gamma_n}$ and increases for $\frac{\partial\sigma(n,\gamma)}{\partial\Gamma_\gamma}$ since this derivative is negative in the neutron energy close to E_0. The two additional peaks of $\frac{\partial\sigma(n,\gamma)}{\partial\Gamma_\gamma}$ decrease in magnitude but they extend their domain into a wider neutron energy region.

Fig. 5 shows the derivatives of the ^{238}U elastic and total cross sections relative to Γ_γ and Γ_n at 293 K for its resonances located at 6.67 eV (Fig. 5 (a)) and 20.871 eV (Fig. 5(b)). It can be noted that the derivatives of the ^{238}U total relative to Γ_γ and the elastic cross sections relative to Γ_n are always positive. Also, it can be noted further that the derivative of the ^{238}U elastic cross section relative to Γ_γ is always negative. Contrary to that, the derivative of the ^{238}U total cross section relative to Γ_γ similarly to $\frac{\partial\sigma(n,\gamma)}{\partial\Gamma_\gamma}$ in Fig. 4(a) shows alternate signs (positive and negative) depending on the neutron energy intervals, it has two additional small peaks and a pronounced dip.

Fig. 6 shows $\frac{\partial\Phi(E)}{\partial\Gamma_\gamma}$ and $\frac{\partial\Phi(E)}{\partial\Gamma_n}$ for the resonances, respectively, located at 6.67 eV (Fig. 6(a)) and at 20.871 eV (Fig. 6(b)). These derivatives were obtained employing Eq. (17). Contrary to the case of $\frac{\partial\sigma^k(E)}{\partial p_l}$ these derivatives do not have a symmetric shape centered in the resonance energy E_0. The antisymmetric effect of the scattering cross section on $\frac{\partial\Phi(E)}{\partial\Gamma_\gamma}$ for the resonance located at 6.67 eV can be observed on the left-hand side of Fig. 6(a). It can be noted a small peak due to the abrupt drop of the scattering cross section in this neutron energy region. As shown in

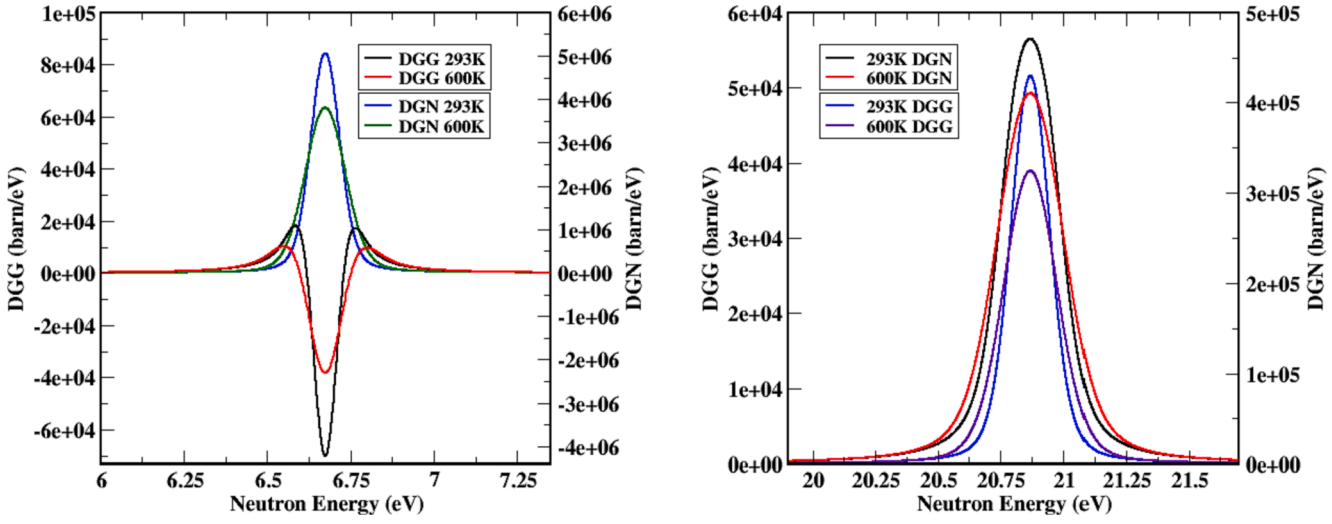

Fig. 4. Derivatives of ^{238}U (n, γ) cross section relative to Γ_γ(DGG) and Γ_n (DGN).

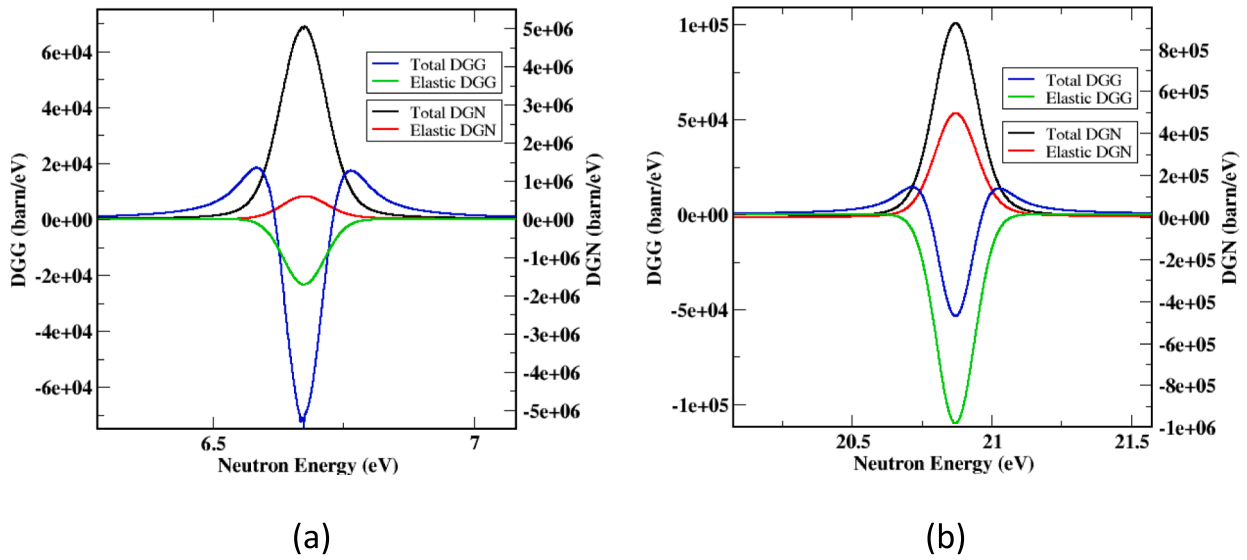

Fig. 5. Derivatives of ^{238}U elastic and total cross section relative to Γ_γ(DGG) and Γ_n (DGN).

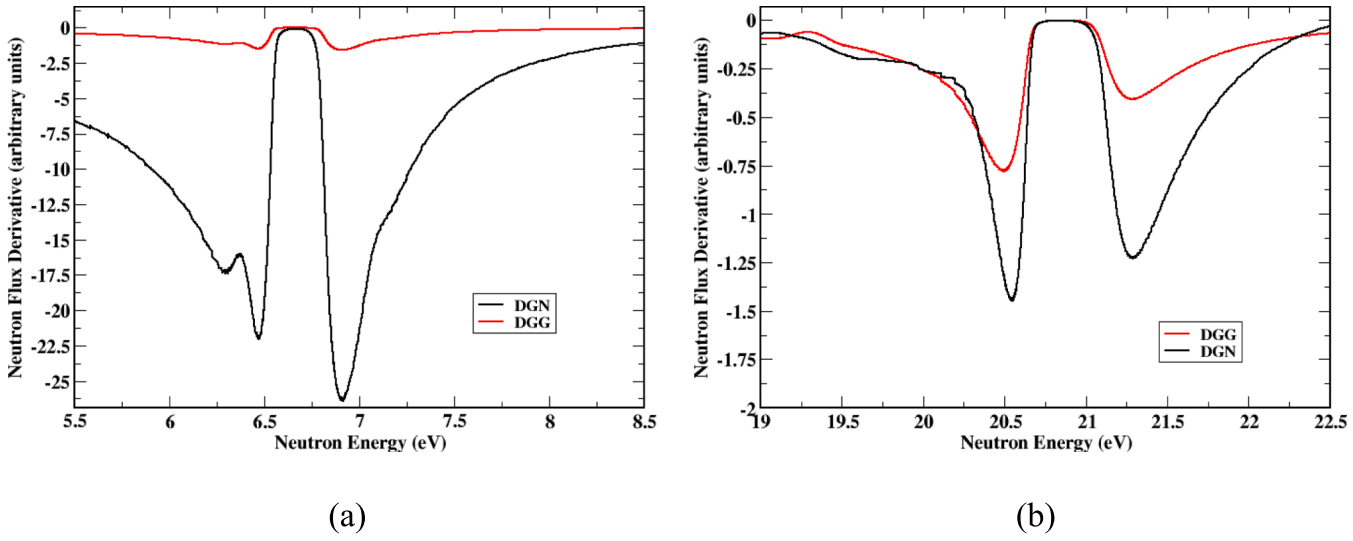

Fig. 6. Neutron flux derivatives relative to Γ_γ(DGG) and Γ_n (DGN).

these figures, these two derivatives are always negative and becomes very close to zero in the neutron energy region close to E_0. This will be the self-shielding effect on the cross sections in the second term of Eq. (15) but now the derivative $\frac{\partial\Phi(E)}{\partial p_i}$ (p_i equal to Γ_γ or Γ_n) is the main agent of this phenomenon. Finally, $\frac{\partial\Phi(E)}{\partial\Gamma_\gamma}$ and $\frac{\partial\Phi(E)}{\partial\Gamma_n}$ have a constraint to go to zero when the neutron energy is far away from the resonance energy. Fig. 6 shows this behavior clearly.

4.2. The determination of the derivatives $\frac{d\sigma_g^k}{dp_i}$

The determination of the derivative of the group cross section to the resonance parameter $\frac{d\sigma_g^k}{dp_i}$ is carried out employing the 2nd and 3rd methodologies as described in Section 3.0. The 2nd methodology involves the substitution of $\frac{\partial\sigma^k(E)}{\partial p_i}$, $\frac{\partial\Phi(E)}{\partial p_i}$, and $\Phi(E)$ in Eq. (15) and the performance of the integrals employing the Simpson rule. The 3rd methodology considers the group cross sections for groups (11) and (15) calculated by ROLAIDS and Eq. (13). In this case $\frac{d\sigma_g^k}{dp_i}$ is calculated in a straightforward fashion employing Eq. (18).

Table 4 shows $\frac{d\sigma_g^k}{dp_i}$ for group (11) employing 2nd Methodology and 3rd Methodology. Here this derivative was calculated at 293 K for the capture, elastic, and total cross sections relative to the resonance parameters Γ_n or Γ_γ. Part 1, Part 2, and Part 3 refer, respectively to the first, second, and third terms of Eq. (15). The nomenclature TOTAL in the fifth column represents the sum of Part 1, Part 2 and Part 3. Initially, note that $\frac{d\sigma_g^k}{dp_i}$ is an additive quantity. The derivative of the total cross section to the resonance parameters is the sum of the corresponding derivatives of the capture and the elastic cross sections. Moreover, a good consistency between the 2nd and 3rd methodologies can be noted according to the small deviation between them shown in last column of Table 4.

According to Eq. (15), Part 1 involves the integral of the product of the derivative $\frac{\partial\sigma^k(E)}{\partial p_i}$ and the neutron flux $\Phi(E)$ in the group energy region under consideration. The neutron flux $\Phi(E)$ is always a positive quantity and consequently the sign of Part1 will depend on the sign of $\frac{\partial\sigma^k(E)}{\partial p_i}$. Fig. 4 (a) shows that the derivative for the ^{238}U neutron capture cross section to Γ_n is always positive and consequently, its Part 1 is also positive. The

Table 4
$\frac{d\sigma_g^k}{dp_i}$: p_i being equal to Γ_n or Γ_γ for groups (11) (293 K).

Reactions	Part 1	Part 2	Part 3	2nd Methodology TOTAL	3rd Methodology ROLAIDS (Reference)	Differences $\frac{(\text{ROLAIDS} - \text{TOTAL})}{\text{ROLAIDS}}$
	(barn/eV)					(%)
Γ_n						
Capture	8106	−6256	1274	3124	3125	−3.20E-02
Elastic	3553	−1932	1407	3028	3028	0.00E + 00
Total	11,659	−8188	2681	6152	6153	−1.63E-02
Γ_γ						
Capture	463.14	–333.84	74.60	203.91	204.17	−1.27E-01
Elastic	−4.21	−110.44	82.40	–32.25	–32.21	1.24E-01
Total	458.94	−444.27	157.00	171.67	171.93	1.51E-01

same does not occur for the derivatives relative to Γ_γ. This derivative as shown in Fig. 4(a) for the neutron capture cross section can assume positive and negative values and the final sign of the integral in group (11) will depend on the competition between its positive and its negative parts. It has been found as shown in Table 4 that the Part 1 is negative only for derivative of the elastic cross section to Γ_γ. All other cross section derivatives relative to Γ_γ are positive.

Part 2 has the integral involving the product of the neutron cross section ($\sigma^k(E)$) and the $\frac{\partial\Phi(E)}{\partial p_i}$ in the neutron group under consideration. The neutron cross section is always a positive quantity and the final value for the sign of Part 2 will depend on the sign of $\frac{\partial\Phi(E)}{\partial p_i}$. Fig. 5(a) shows that the sign of $\frac{\partial\Phi(E)}{\partial p_i}$ is always negative and consequently the sign of Part 2, as shown in Table 4, will be negative independently of the neutron reaction type and the resonance parameter under consideration. The same reasoning applies to Part 3 but in this case the integral involves only $\frac{\partial\Phi(E)}{\partial p_i}$. As stated, $\frac{\partial\Phi(E)}{\partial p_i}$ is always negative but there is a minus sign in the third term of Eq. (15) (Part 3) and therefore, as shown in Table 4, Part 3 will be always positive independently of the neutron reaction type and the resonance parameter considered since all other quantities that multiply the integral are positive. The final sign for $\frac{d\sigma_g^k}{dp_i}$ will depend on the competition of the sum of these three parts. The same reasoning applies to group (15). In this case the considerations previously made for the signs of $\frac{\partial\sigma^k(E)}{\partial p_i}$ have to be taken into consideration.

Table 5 shows show, respectively $\frac{d\sigma_g^k}{d\Gamma_n}$ and $\frac{d\sigma_g^k}{d\Gamma_\gamma}$ for groups (11) and (15) as a function of temperature. These data along with their uncertainties are shown in a graphical form in Figs. 7 and 8. These results were based on the 3rd Methodology; (ROLAIDS). The uncertainties in these derivatives due to the NJOY linearization and Doppler Broadening precisions are estimated to be ~ 1.2%. Initially, according to Figs. 7 and 8 for the same group and resonance parameter the capture and total cross section derivatives have a similar shape. Also, Figs. 7 and 8 show that with exception to the derivative of the scattering cross section relative to Γ_γ in group (15) all other derivatives are positive and increase from 0 to 293 K. Particularly, the derivative of the scattering cross section relative to Γ_n in group (11) stays closely inside of the 1-σ range of the calculated uncertainty. $\frac{d\sigma_{11}^k}{d\Gamma_n}$ for the capture and total cross sections stays nearly constant between 293 and 900 K and then shows a sharp increase. $\frac{d\sigma_{15}^k}{d\Gamma_\gamma}$ for the capture and total cross section increases steadily up to 900 K and then decreases at 1200 K. Conversely, the derivative of the scattering cross section to Γ_γ in group (15) stays nearly inside of the 1-σ range of the calculated uncertainty from 293 K to 900 K and then decreases at 1200 K. The data on Table 5 will be employed subsequently for the determination of the multigroup covariance matrix.

Table 5
$\frac{d\sigma_g^k}{dp_i}$: p_i being equal to Γ_n or Γ_γ as a function of temperature for groups (11) and (15) (barn/eV).

Group	Reactions	Temperature (K)				
		0	293	600	900	1200
11		**Neutron Width** (Γ_n)				
	Capture	2955	3158	3174	3231	3579
	Elastic	3063	3037	2995	2949	3034
	Total	6017	6195	6170	6180	6614
		Gamma Width (Γ_γ)				
	Capture	190.40	203.23	222.02	228.97	202.40
	Elastic	–32.70	–33.25	−34.12	–32.97	−41.36
	Total	157.70	169.98	187.93	196.03	161.04
15		**Neutron Width** (Γ_n)				
	Capture	514.39	537.47	532.83	521.79	482.33
	Elastic	427.76	422.53	437.58	429.63	407.80
	Total	942.14	960.00	970.37	951.35	890.06
		Gamma Width (Γ_γ)				
	Capture	223.27	225.61	223.95	219.83	214.80
	Elastic	−73.96	−75.18	−77.24	−79.86	−83.00
	Total	149.31	150.47	146.73	139.96	131.82

4.3. *The self-shielding factors for* $\frac{d\sigma_g^k}{dp_i}$

The resonance self-shielding phenomenon is classic in thermal reactors fueled with slightly enriched uranium and occurs due to the neutron flux depression in the neutron energies close to the thermal and epithermal energy region. Fig. 6 shows this phenomenon for the unit cell of the IPEN/MB-01 reactor in the first innermost zone of the UO_2 fuel. It is clearly seen the "dips" of the neutron flux in the neutron energy regions close to the resonance energies E_0.

In the classical case of the determination of the multigroup cross sections as given by Eq. (13) the quantities involved: cross sections and neutron flux both as a function of the neutron energy are positive quantities and necessarily the multigroup cross section resulting from this equation will also be positive. The self-shielding effects on the cross sections are already implicit when the integrals are performed.

The self-shielding phenomenon in the multigroup covariance matrices is much more complex. Consider the three Parts of Eq. (15). The first one involves the product of the derivative $\frac{\partial\sigma^k(E)}{\partial p_i}$ and the neutron flux $\phi(E)$. The second term involves the product of the cross section $\sigma^k(E)$ and the derivative of the neutron flux $\frac{\partial\Phi(E)}{\partial\Gamma_\gamma}$. The third term just involves $\frac{\partial\Phi(E)}{\partial\Gamma_\gamma}$. The resonance self-shielding effects occur in all these three terms when the integrals in the energy group under consideration are performed.

Consider group (11) where the ^{238}U resonance located at 6.67 eV plays a major role. Fig. 9 illustrates the self-shielding phenomenon occurring in Part 1 (Fig. 9 (a)) and Part 2 (Fig. 9 (b)) of Eq. (15). Fig. 9 (a) shows the derivative of ^{238}U (n, γ) cross section relative to Γ_γ(DGG) and the neutron flux $\Phi(E)$ at 293 K. In this case, the self-shielding effect

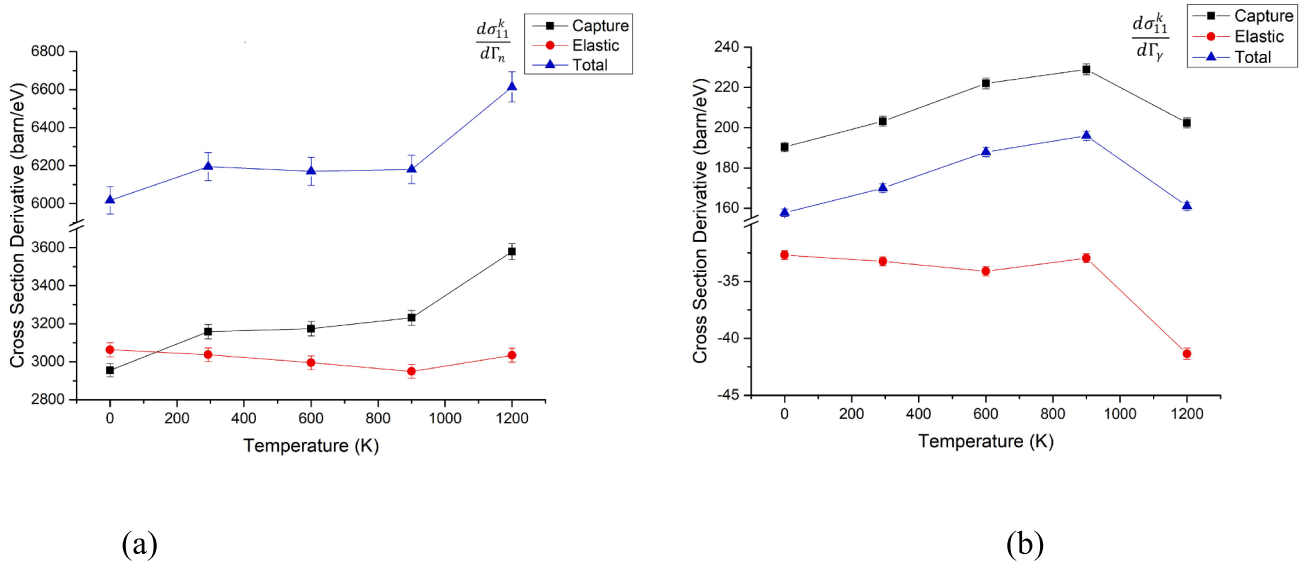

Fig. 7. $\frac{d\sigma_{11}^k}{d\Gamma_n}$ (a) and $\frac{d\sigma_{11}^k}{d\Gamma_\gamma}$ (b) as a function of temperature.

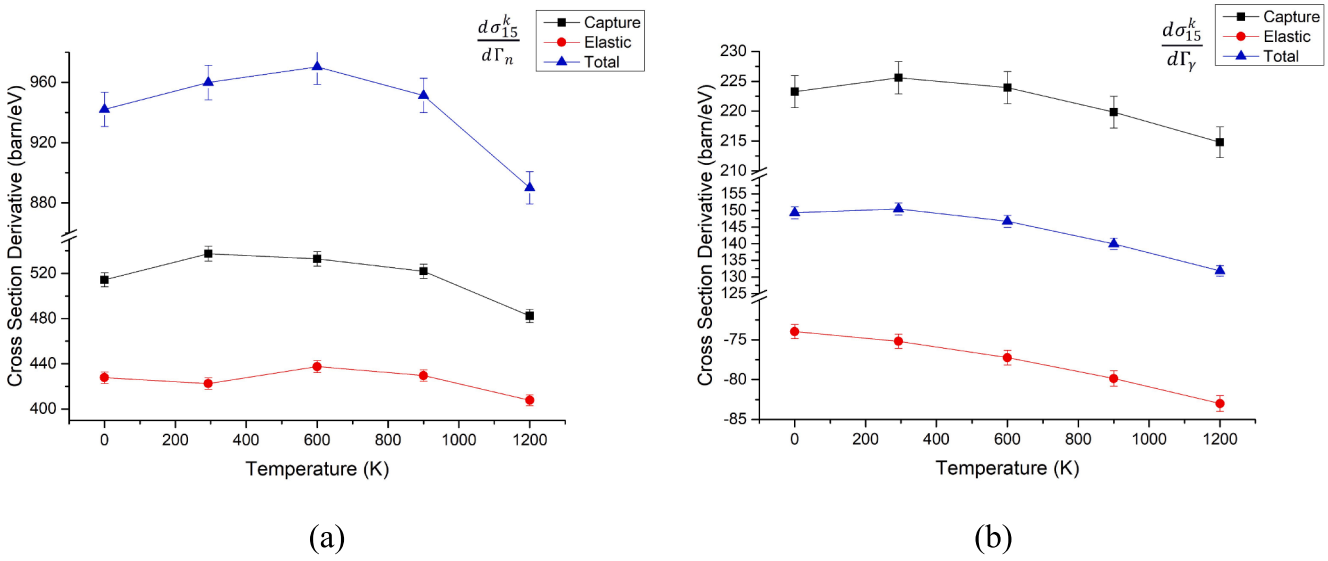

Fig. 8. $\frac{d\sigma_{15}^k}{d\Gamma_n}$ (a) and $\frac{d\sigma_{15}^k}{d\Gamma_\gamma}$ (b) as a function of temperature.

in this derivative is clearly seen for the neutron energy region where this quantity is negative. The magnitude of the neutron flux goes to zero sharply and the derivative of the ^{238}U (n, γ) cross section relative to Γ_γ shows a sharp drop. When the integrals in the energy group (11) are performed these effects mostly cancel each other. However, for the positive region of DGG where the two peaks are present the self-shielding is not so evident. The net effect when the integral of Part 1 of Eq. (23) is performed will depend on the competition between positive and negative regions of this ^{238}U (n, γ) derivative.

Fig. 9 (b) shows the ^{238}U total cross section and $\frac{\partial\Phi(E)}{\partial\Gamma_\gamma}$, both as a function of neutron energy for group (11) at 293 K. $\frac{\partial\Phi(E)}{\partial\Gamma_\gamma}$ is negative in the whole neutron energy interval of group (11) and goes to zero far away from the resonance energy. Here, the self-shielding in the total cross section is similar to the classical case but the weighting function is $(\frac{\partial\Phi(E)}{\partial\Gamma_\gamma})$ which is always negative. The self-shielding in the ^{238}U total cross section is more pronounced and noticeable in the neutron energy region close to the resonance peak since $\frac{\partial\Phi(E)}{\partial\Gamma_\gamma}$ although negative goes nearly to zero in this region. The others ^{238}U neutron reactions (capture and elastic scattering) follow the same pattern. This is the self-shielding phenomenon occurring in Part 2 of Eq. (23).

The third term of Eq. (23) considers only the integral of $\frac{\partial\Phi(E)}{\partial\Gamma_\gamma}$ in the group under consideration. Here, the derivative $\frac{\partial\Phi(E)}{\partial\Gamma_\gamma}$ was already affected by the presence of the resonance as discussed previously and the self-shielding affects affect only the integral of this quantity.

The resonance self-shielding phenomenon is mathematically quantified defining the self-shielding factor F_{SF} (Zhang et al., 2015). Like the classical case of the cross section, the self-shielding factor for the derivative $\frac{d\sigma_g^k}{dp_i}$ can be defined as:

$$F_{SF} = \frac{\frac{d\sigma_g^k}{dp_i}\boldsymbol{calculatedatfinitedilution}}{\frac{d\sigma_g^k}{dp_i}\boldsymbol{calculatedatinfinitedilution}} \quad (22)$$

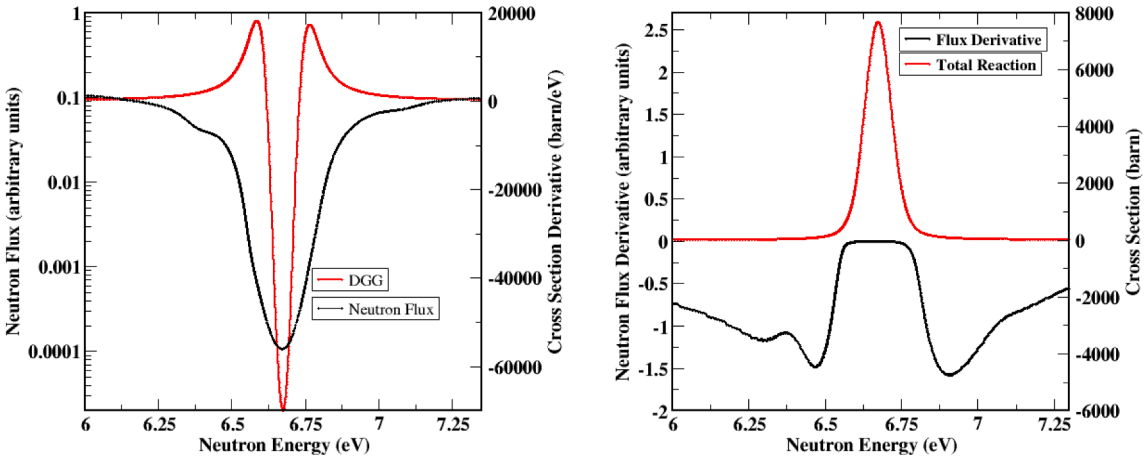

(a) Derivative of ^{238}U (n, γ) cross section relative to Γ_γ (DGG) and $\Phi(E)$ from ROLAIDS

(b) Derivative of the neutron flux relative to Γ_γ and the ^{238}U total cross section at 293K

Fig. 9. Origin of the self-shielding effects on the multigroup covariance matrix.

where the notation " *finitedilution*" means that the derivative $\frac{d\sigma_g^k}{dp_i}$ was calculated by employing the neutron flux and its derivative at the nominal values of the nuclide density of the nuclide under consideration. In the case of the IPEN/MB-01 unit cell the nominal value of the ^{238}U nuclide density is the value specified in its benchmark model (2.1694E-02 atom/barn-cm). The notation " *infinitedilution*" means that the nuclide density of the nuclide under consideration is so small that the solution for the neutron flux is C/E, where C is an arbitrary constant and E is the neutron energy. In this case all the neutron flux derivatives in Eq. (15) goes to zero. The self-shielding factor is a measure of the importance of the resonance self-shielding effects. The smaller this factor if positive and higher if negative the more important is the resonance self-shielding effects.

Table 6 shows the derivative $\frac{d\sigma_g^k}{dp_i}$ and its self-shielding factors employing the 3rd methodology (ROLAIDS) at 293 K. This table shows $\frac{d\sigma_g^k}{dp_i}$ for group (11) at the nominal ^{238}U atomic density and at the infinite dilution, and the corresponding self-shielding factor employing Eq. (22). In a general sense, Table 6 reveals that the self-shielding effects factor are considerable and need to be take into account in the uncertainty analyses. Also, the self-shielding factor for the total cross section is not the sum of the self-shielding factors of the capture and elastic cross sections. As shown in Table 6, all the derivatives relative to Γ_n (including the infinite dilution) are positive and so are their self-shielding factors. Here, the derivative of elastic cross section relative to Γ_n has the largest self-shielding factor due to its large infinite dilution value. The derivative of the elastic cross section relative to Γ_γ both at the finite and infinite dilution is negative what makes its self-shielding factor positive. The same did not occur for the derivative of the total cross section relative do Γ_γ. Its finite dilution value is positive, but its infinite dilution value is negative making its self-shielding factor negative. This fact is very surprising and impossible to occur in the classical cross section self-shielding treatment.

Table 6
$\frac{d\sigma_g^k}{dp_i}$ and its self-shielding factors for group (11). (293 K).

Reactions	$\frac{d\sigma_g^k}{dp_i}$ 3rd Methodology Finite Dilution	$\frac{d\sigma_g^k}{dp_i}$ Infinite Dilution	Self-Shielding Factor
	(barn/eV)		(dimensionless)
Γ_n			
Capture	3158	327,780	0.0095
Elastic	3037	45,145	0.0673
Total	6195	372,924	0.0165
Γ_γ			
Capture	203.23	825.04	0.2457
Elastic	−33.25	−1386.33	0.0239
Total	169.98	−561.39	−0.3022

Figs. 10 and 11 show the self-shielding factors as a function of temperature, respectively for groups (11) and (15). The temperatures considered are 0 K, 293 K, 600 K, 900 K, and 1200 K and the self-shielding factors are shown for the derivatives of the capture, elastic, and total cross sections relative to either Γ_n or Γ_γ. These figures show that the self-shielding effects although not strongly are temperature dependent. The same conclusions reached in Table 6 can be extended to these figures but now the self-shielding factor for the derivative of the total cross section relative to Γ_γ for group (15) besides of being negative has its absolute value higher than 1. Also here, this fact is very surprising and can not be obtained with the classical cross section self-shielding.

Figs. 10 and 11 reveals that the self-shielding factors have the same behavior as their corresponding derivative only for $\frac{d\sigma_{15}^k}{d\Gamma_n}$. The self-shielding factor for $\frac{d\sigma_{11}^k}{d\Gamma_n}$ has its largest value for the elastic cross section for the reasons already mentioned. This derivative decreases up to 900 K and then increases. The $\frac{d\sigma_{11}^k}{d\Gamma_n}$ self-shielding factor for the capture and total cross section increases slowly from 0 to 1200 K. The $\frac{d\sigma_{11}^k}{d\Gamma_\gamma}$ self-shielding factor for the capture cross section shows similar trends in groups (11) and (15). It increases up to a maximum value and then decreases. The maximum value for group (11) occurs at 900 K while that for group (15) at 293 K. The $\frac{d\sigma_{11}^k}{d\Gamma_\gamma}$ self-shielding for the elastic and total cross section in group (11) remain nearly close to the 1-σ range of the calculated uncertainty up to 900 K and then increases. The $\frac{d\sigma_{15}^k}{d\Gamma_\gamma}$ self-shielding for the elastic cross section increases steadily form 0 to 1200 K while that for the total cross section remains nearly close to the 1-σ range of the calculated uncertainty up to 900 K and then increases.

4.4. Numerical results for the multigroup cross section covariance matrix

The elements of the multigroup cross section covariance matrix

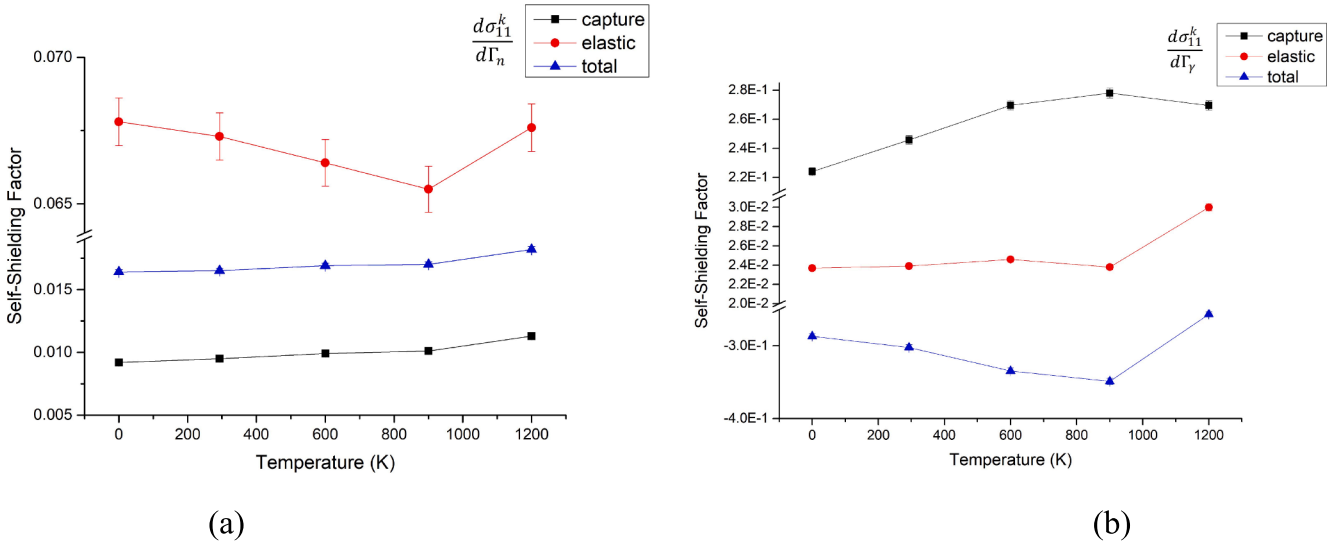

Fig. 10. Self-shielding factors for $\frac{d\sigma_{11}^k}{d\Gamma_n}$ (a) and $\frac{d\sigma_{11}^k}{d\Gamma_\gamma}$ (b) as a function of temperature.

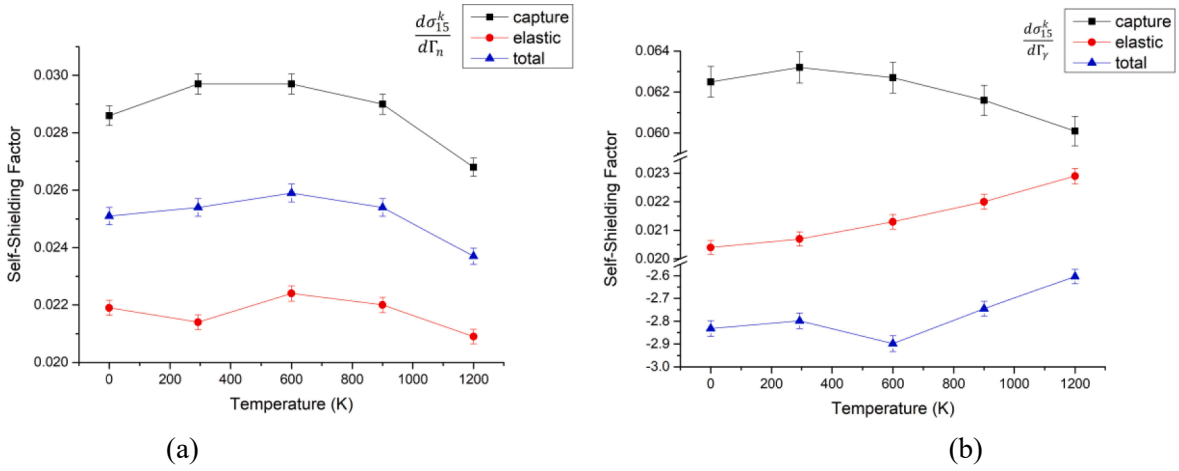

Fig. 11. Self-shielding factors for $\frac{d\sigma_{15}^k}{d\Gamma_n}$ (a) and $\frac{d\sigma_{15}^k}{d\Gamma_\gamma}$ (b) as a function of temperature.

(ENDF FILE 33) are defined by Eq. (12). Since the matrix of the covariance of the resonance parameters given in Table 2 is diagonally symmetric the same will occur for the multigroup cross section covariance matrix. According to Eq. (12) and (Leal et al, 2005) the elements of the multigroup cross section covariance matrix for the groups (11) ($\Theta_{11,11}^k$) and 15 ($\Theta_{15,15}^k$) and their non-diagonal element ($\Theta_{11,15}^k$) are given by:

$$\Theta_{11,11}^k = \frac{d\sigma_{11}^k}{d\Gamma_\gamma^1} < \Gamma_\gamma^1, \Gamma_\gamma^1 > \frac{d\sigma_{11}^k}{d\Gamma_\gamma^1} + 2 \bullet \frac{d\sigma_{11}^k}{d\Gamma_\gamma^1} < \Gamma_\gamma^1, \Gamma_n^1 > \frac{d\sigma_{11}^k}{d\,\Gamma_n^1} + \frac{d\sigma_{11}^k}{d\,\Gamma_n^1} < \Gamma_n^1, \Gamma_n^1 > \frac{d\sigma_{11}^k}{d\,\Gamma_n^1} \tag{23}$$

$$\Theta_{15,15}^k = \frac{d\sigma_{15}^k}{d\Gamma_\gamma^2} < \Gamma_\gamma^2, \Gamma_\gamma^2 > \frac{d\sigma_{15}^k}{d\Gamma_\gamma^2} + 2 \bullet \frac{d\sigma_{15}^k}{d\Gamma_\gamma^2} < \Gamma_\gamma^2, \Gamma_n^2 > \frac{d\sigma_{15}^k}{d\Gamma_n^2} + \frac{d\sigma_{15}^k}{d\Gamma_n^2} < \Gamma_n^2, \Gamma_n^2 > \frac{d\sigma_{15}^k}{d\Gamma_n^2} \tag{24}$$

and

$$\Theta_{11,15}^k = 2 \bullet \frac{d\sigma_{11}^k}{d\Gamma_\gamma^1} < \Gamma_\gamma^1, \Gamma_\gamma^2 > \frac{d\sigma_{15}^k}{d\Gamma_\gamma^2} + 2 \bullet \frac{d\sigma_{15}^k}{d\Gamma_\gamma^2} < \Gamma_\gamma^2, \Gamma_n^1 > \frac{d\sigma_{11}^k}{d\Gamma_\gamma^1} +$$

$$2 \bullet \frac{d\sigma_{11}^k}{d\Gamma_\gamma^1} < \Gamma_\gamma^1, \Gamma_\gamma^2 > \frac{d\sigma_{15}^k}{d\Gamma_\gamma^2} + 2 \bullet \frac{d\sigma_{15}^k}{d\Gamma_\gamma^2} < \Gamma_\gamma^2, \Gamma_\gamma^1 > \frac{d\sigma_{11}^k}{d\Gamma_\gamma^1} \tag{25}$$

where the Γ superscripts 1 and 2, refer respectively to the first and second ^{238}U resonance located at 6.67 eV and 20.871 eV.

The derivatives $\frac{d\sigma_g^k}{dp_i}$ needed to obtain $\Theta_{11,11}^k$, $\Theta_{15,15}^k$, and $\Theta_{11,15}^k$ arises from Table 5 for groups (11) and (15) and the elements of the resonance parameter covariance matrix from Table 2. Eqs. (23) and (24) are the diagonal elements of the multigroup covariances, respectively, for groups (11) and (15). These diagonal elements are the variance of the corresponding group cross section and the uncertainties of them can be found as the square root of their variances. Consequently, $\Theta_{11,11}^k$ and $\Theta_{15,15}^k$ must assume positive values.

Consider initially Eq. (23). This equation is made of three terms and each one of them contains a triple product involving two derivatives $\frac{d\sigma_g^k}{dp_i}$ and one element of the resonance parameter covariance matrix. The analyses of these terms are important to illustrate the impact of the

correlated and uncorrelated elements of the resonance parameter covariance matrix on the elements of the multigroup covariance matrix. Table 7 shows these three terms for the capture, elastic, and total cross sections as a function of temperature for group (11). The components of the resonance parameter covariance matrix for group (11) as given in Table 2 are all positive and consequently, independently of the type of the cross section considered, the first and third term of Eq. (23) are necessarily positive because they are the result of the product of the square of the derivatives and the variance of the resonance parameter. The second term involves a crossed term which will depend on the sign of the product between $\frac{d\sigma_{11}^k}{d\Gamma_\gamma^1}$ and $\frac{d\sigma_{11}^k}{d\Gamma_n^1}$. According to Table 5, $\frac{d\sigma_{11}^k}{d\Gamma_\gamma^1}$ is always positive and $\frac{d\sigma_{11}^k}{d\Gamma_n^1}$ is negative only for the scattering cross section. Consequently, the second term of Eq. (23) will be positive for the capture and total cross sections and negative for the scattering cross section. Finally, it must be realized that the sum of the three terms for $\Theta_{11,11}^k$ must be, independently of the cross section considered, positive since they represent, respectively, the variance of the corresponding group cross sections.

The same analysis can be applied to group (15) given by Eq. (24) but note that in this case the sign of $\frac{d\sigma_{15}^k}{d\Gamma_n^2}$ and $\frac{d\sigma_{15}^k}{d\Gamma_\gamma^2}$ follows the same pattern of group (11), and that the covariance for the crossed term involving Γ_n^2 and Γ_γ^2 is negative (anti-correlated). Consequently, the second term of Eq. (24) will be negative for the capture and total cross sections and positive for the elastic. The final value of $\Theta_{15,15}^k$ will depend on the competition between the three terms in Eq. (24) but its final value must be positive.

The analyses of the non-diagonal element of the multigroup covariance matrix given by Eq. (25) is more complicated due to the correlation between the resonance parameters of the resonance present in groups (11) and (15). The final result is that their capture cross section elements are anti correlated and the elastic and total cross sections are correlated.

Table 8 shows the temperature dependence of the multigroup covariance matrix for group (15) and the crossed element 11–15. In general, the elements of the multigroup cross section covariance matrix changes with the temperature and it can not be neglected in the uncertainty analyses of the integral responses of nuclear reactors. A good example of that is the determination of the uncertainties of the Doppler coefficients like that shown in (Otuka et al., 2008). The treatment of the temperature dependence of all kinds of sources of uncertainties is crucial in this case.

Finally, it must be noted that the elements of the cross section correlation matrix for the total reaction rate is not equal to the sum to those of the capture and elastic reaction rates.

Table 8
Elements of the multigroup covariance matrix (barn^2).

	Reactions	Temperature (K)				
		0	293	600	900	1200
$\Theta_{15,15}^k$	Capture	0.1003	0.0995	0.0980	0.0946	0.0959
	Elastic	1.1259	1.1182	1.1934	1.1885	1.1373
	Total	1.0272	1.0802	1.1481	1.1361	0.9875
$\Theta_{11,15}^k$	Capture	−0.0393	−0.0386	−0.0405	−0.0410	−0.0457
	Elastic	0.0519	0.0510	0.0515	0.0509	0.0486
	Total	0.1318	0.1420	0.1534	0.1567	0.1426

4.4.1. Resonance self-Shielding factors for the elements of the multigroup covariance matrix

The self-shielding factors for the elements of the multigroup covariance matrices as a function of temperature are shown in Table 9. This table shows that in a general sense the self-shielding effects in the multigroup covariance matrices are severe and they must be taken into consideration in the uncertainty analyses of reactor responses. The self-shielding-factors depends on the reaction type, but for the same reaction type they are weakly dependent on the temperature. It must be noted in Table 9 that the self-shielding factor for $\Theta_{11,15}^k$ is negative for the capture cross section. This finding makes the impact of the self-shielding phenomenon on the determination of the uncertainties of integral responses even more complicated and difficult to interpret.

4.4.2. Comparisons of the 1st methodology (NJOY) to the 2nd and 3rd methodologies

There are two major differences between the 1st methodology (NJOY) and the methodologies developed in this work. First, the ERRORR module of NJOY employs the Breit-Wigner formalism (Breit and Wigner, 1936) at 0 K to calculate the derivative of the cross sections to the resonance parameters and second ERRORR considers only the direct effect (PART 1 of Eq. (15)) for the determinations of the derivatives of the multigroup cross section relative to the resonance parameters and consequently the multigroup covariance matrix. Particularly, the second difference is by far the most important and it will impose severe restrictions to the multigroup covariance matrices generated by NJOY.

Table 10 shows the comparison of the of the covariance matrix results for group (11) at 0 K and 293 K between 1st methodology (NJOY) to those of the 2nd (PART 1) and 3rd methodologies. Initially, note that the NJOY result changes from 0 K to 293 K are due to the temperature changes of the ROLAIDS weighting flux. Table 10 reveals that the NJOY results at 0 K are very close to the ones of the PART1 of the 2nd methodology. The same does not occur at 293 K for the reasons already mentioned. The relatively high discrepancy between NJOY and PART1

Table 7
Multigroup covariance matrix components for group (11) (barn^2).

Reactions	Partial Terms	Temperature (K)				
		0	293	600	900	1200
Capture	1st Term	0.0080	0.0091	0.0092	0.0096	0.0117
	2nd Term	0.0190	0.0216	0.0238	0.0250	0.0244
	3rd Term	0.0112	0.0128	0.0153	0.0162	0.0127
	$\Theta_{11,11}^k$	0.0382	0.0435	0.0483	0.0508	0.0478
Elastic	1st Term	0.0086	0.0084	0.0082	0.0080	0.0084
	2nd Term	−0.0033	−0.0034	−0.0034	−0.0032	−0.0042
	3rd Term	0.0003	0.0003	0.0003	0.0003	0.0005
	$\Theta_{11,11}^k$	0.0055	0.0054	0.0051	0.0051	0.0047
Total	1st Term	0.0333	0.0353	0.0350	0.0351	0.0402
	2nd Term	0.0320	0.0355	0.0391	0.0409	0.0359
	3rd Term	0.0077	0.0089	0.0109	0.0119	0.0080
	$\Theta_{11,11}^k$	0.0730	0.0797	0.0850	0.0879	0.0841

Table 9
Self-Shielding factors for $\Theta^k_{11,11}$, $\Theta^k_{11,15}$, $\Theta^k_{15,15}$.

Matrix Element	Reaction	Temperature (K)				
		0	293	600	900	1200
$\Theta^k_{11,11}$	Capture	0.00036	0.00040	0.00046	0.00049	0.00048
	Elastic	0.01553	0.01511	0.01441	0.01415	0.01348
	Total	0.00062	0.00065	0.00073	0.00076	0.00074
$\Theta^k_{15,15}$	Capture	0.00036	0.00035	0.00035	0.00034	0.00034
	Elastic	0.00045	0.00045	0.00048	0.00048	0.00046
	Total	0.00024	0.00025	0.00027	0.00026	0.00023
$\Theta^k_{11,15}$	Capture	−0.00056	−0.00053	−0.00058	−0.00059	−0.00066
	Elastic	0.00263	0.00257	0.00261	0.00259	0.00249
	Total	0.00032	0.00036	0.00037	0.00034	0.00032

Table 10
Covariance matrix values for groups (11) at 0 K and 293 K.

	Reaction	NJOY (barn^2)	2nd Methodology (Part 1) (barn^2)	Difference $\frac{(\text{NJOY}-\text{Part 1})}{\text{Part 1}}$(%)	3rd Methodology (ROLAIDS) (barn^2)	Difference $\frac{(\text{NJOY}-\text{ROLAIDS})}{\text{ROLAIDS}}$(%)
0 K	Capture	2.986E-01	2.988E-01	−8.93E-02	3.831E-02	6.79E + 02
	Elastic	1.957E-02	1.164E-02	6.81E + 01	5.588E-03	2.50E + 02
	Total	3.935E-01	4.282E-01	−8.11E + 00	7.315E-02	4.38E + 02
293 K	Capture	2.117E-01	2.539E-01	−1.66E + 01	4.370E-02	3.84E + 02
	Elastic	1.882E-02	1.119E-02	6.82E + 01	5.426E-03	2.47E + 02
	Total	2.894E-01	3.717E-01	−2.21E + 01	7.991E-02	2.62E + 02

for the elastic cross section at 0 K may be due to the treatment of the anti-symmetric term in the Breit-Wigner model. It appears that NJOY neglect that. The differences between NJOY and 3nd methodology (ROLAIDS) results are severe and exceeding hundreds of percent. This occurred mainly for the non-treatment of the indirect effects due to the neutron flux in the multigroup cross section derivatives.

Table 11 shows the comparison of the elements of the multigroup covariance matrices as a function of the temperature produced by NJOY and ROLAIDS. The comparison is expressed as (NJOY −ROLAIDS)/ROLAIDS in units of %. The differences between NJOY and ROLAIDS methodologies are severe and like that already discussed in Table 11.

Table 11
Comparison (NJOY – ROLAIDS in %) for $\Theta^k_{11,11}$, $\Theta^k_{15,15}$, and $\Theta^k_{11,15}$(%).

Matrix Element	Reaction	Temperature (K)				
		0	293	600	900	1200
$\Theta^k_{11,11}$	Capture	6.79E + 02	3.84E + 02	2.31E + 02	1.59E + 02	1.36E + 02
	Elastic	2.50E + 02	2.47E + 02	2.52E + 02	1.18E + 02	2.67E + 02
	Total	4.38E + 02	2.62E + 02	1.66E + 02	1.18E + 02	1.02E + 02
$\Theta^k_{15,15}$	Capture	2.61E + 02	1.57E + 02	1.07E + 02	8.00E + 01	5.31E + 01
	Elastic	2.76E + 01	4.52E + 00	2.69E + 01	3.81E + 01	4.37E + 01
	Total	4.03E + 01	2.53E + 00	1.95E + 01	3.02E + 01	2.91E + 01
$\Theta^k_{11,15}$	Capture	1.69E + 02	8.61E + 01	3.41E + 01	7.50E + 00	1.80E + 01
	Elastic	3.15E + 02	2.90E + 02	2.71E + 02	2.59E + 02	2.57E + 02
	Total	1.16E + 02	1.19E + 02	1.21E + 02	1.21E + 02	1.24E + 02

4.5. The results of the 4th methodology (MCNP6) and ROLAIDS comparisons

All MCNP6 runs considered the kcode option with 3 million histories per cycle and a total of 4500 cycles. The first 50 cycles were skipped. The maximum relative standard deviation achieved was 0.0001 for all tallies and neutron group considered. In this case the perturbations in the resonance parameters had to be higher than that for the 2nd and 3rd methodologies A perturbation in the resonance parameters of 1% was found adequate to attend first order approximation and to get good estimates for the derivative $\frac{d\sigma^k_g}{dp_i}$. This derivative was calculated employing Eq. (20) in conjunction with the group cross sections from Eq. (19). The procedure to get the multigroup covariance matrix is the same as that employed in the 3rd methodology.

Consider initially the comparison of $\frac{d\sigma^k_g}{dp_i}$. Tables 13 and 14 show the comparison of the MCNP6 results to those of the 3rd methodology (ROLAIDS). The ROLAIDS results employed Eqs. (21) and (20) to be consistent to those of MCNP6. The comparison here also verifies if the infinite array of unit cell model employed by ROLAIDS against the explicit 3D model employed by MCNP6 is adequate. Tables 12 and 13 show the comparison of ROLAIDS and MCNP6 for the derivative $\frac{d\sigma^k_g}{dp_i}$ and for the multigroup covariance matrix, respectively. Tables 12 and 13 reveals that the agreement between the ROLAIDS and MCNP6 results can be considered very good and supports the whole developments performed and the conclusions reached in this work to obtain the multigroup covariance matrices. The maximum deviation was reached for $\frac{d\frac{d\sigma^5_g}{dp_i}}{d\Gamma_\gamma}$ which shows a discrepancy of nearly 6% for group (15) but it does not compromise the main achievements of this work.

4.6. The IPEN/MB-01 k_{eff} reactor uncertainty analyses

The IPEN/MB-01 critical configuration described in Section 4.4.3 is employed as an example for the application of the multigroup covariance matrix methodologies developed in this paper. The aim here is performed the k_{eff} uncertainty analyses of this critical configuration. The

Table 12

ROLAIDS and MCNP6 $\frac{d\sigma_g^k}{dp_i}$ comparisons.

Group	Reaction	**Gamma Width** (Γ_γ)			**Neutron Width** (Γ_n)		
		MCNP6	ROLAIDS	Difference	MCNP6	ROLAIDS	Difference
		(barn/eV)		(%)	(barn/eV)		(%)
11	Capture	434.61	445.85	2.52	6813.54	6658.03	2.33
	Elastic	−51.93	−52.41	0.91	3956.79	3966.98	0.25
15	Capture	370.18	370.30	−0.03	774.38	769.39	0.65
	Elastic	−129.68	−121.88	6.40	813.29	799.96	1.67

Table 13

ROLAIDS and MCNP6 comparison of the elements of the multigroup covariance matrix (barn^2).

Element	Reaction	MCNP5	ROLAIDS	Difference (%)
$\Theta^k_{11,11}$	Capture	0.2015	0.2028	−0.68
	Elastic	0.0083	0.0083	−0.09
$\Theta^k_{15,15}$	Capture	0.3230	0.3277	−1.43
	Elastic	3.8793	3.6573	6.07
$\Theta^k_{11,15}$	Capture	−0.1864	−0.1895	−1.63
	Elastic	0.1172	0.1166	0.52

procedure employs mostly the fourth methodology based on MCNP6 and the 3-D IPEN/MB-01 benchmark model described in Sections 4.4.3 and 3.0. The uncertainty analyses are restricted to the uncertainties of the first two ^{238}U resonances already discussed. Two distinct approaches are developed to cope with this task.

The first approach considers k_{eff} as the integral reactor response R in Eq. (1) and the parameter $p(E)$ are the resonance parameters Γ_n and Γ_γ for the two ^{238}U resonances. According to Eq. (1) and noting that the variance $V(R)$ is equal to $(\sigma_R)^2$, the k_{eff} uncertainty can be found as:

$$\left(\sigma_{k_{eff}}\right)^2 = V^{11}_{k_{eff}} + V^{22}_{k_{eff}} + 2 \bullet V^{12}_{k_{eff}} \tag{26}$$

where

$$V^{11}_{k_{eff}} = \frac{dk_{eff}}{d\Gamma^1_n} < \Gamma^1_n, \Gamma^1_n > \frac{dk_{eff}}{d\Gamma^1_n} + \frac{dk_{eff}}{d\Gamma^1_n} < \Gamma^1_\gamma, \Gamma^1_\gamma > \frac{dk_{eff}}{d\Gamma^1_\gamma} + 2 \bullet \frac{dk_{eff}}{d\Gamma^1_n} < \delta\Gamma^1_n, \Gamma^1_\gamma > \frac{dk_{eff}}{d\Gamma^1_\gamma} \tag{27}$$

$$V^{22}_{k_{eff}} = \frac{dk_{eff}}{d\Gamma^1_n} < \Gamma^2_n, \Gamma^2_n > \frac{dk_{eff}}{d\Gamma^2_n} + \frac{dk_{eff}}{d\Gamma^2_n} < \Gamma^2_\gamma, \Gamma^2_\gamma > \frac{dk_{eff}}{d\Gamma^2_\gamma} + 2 \bullet \frac{dk_{eff}}{d\Gamma^2_n} < \Gamma^2_n, \Gamma^2_\gamma > \frac{dk_{eff}}{d\Gamma^2_\gamma} \tag{28}$$

$$V^{12}_{k_{eff}} = \frac{dk_{eff}}{d\Gamma^1_n} < \Gamma^1_n, \Gamma^2_n > \frac{dk_{eff}}{d\Gamma^2_n} + \frac{dk_{eff}}{d\Gamma^1_n} < \Gamma^1_n, \Gamma^2_\gamma > \frac{dk_{eff}}{d\Gamma^2_\gamma} + \frac{dk_{eff}}{d\Gamma^1_\gamma} < \Gamma^1_\gamma, \Gamma^2_n > \frac{dk_{eff}}{d\Gamma^2_n} + \frac{dk_{eff}}{d\Gamma^1_\gamma} < \Gamma^1_\gamma, \Gamma^2_\gamma > \frac{dk_{eff}}{d\Gamma^2_\gamma} \tag{29}$$

and $\frac{dk_{eff}}{d\Gamma^1_n}$ represents the k_{eff} derivative to Γ^1_n and so on, and the superscripts "1″ and "2" in Γ_n and Γ_γ have the same meaning as before.

The k_{eff} derivatives to the resonance parameters Γ_n and Γ_γ; here symbolized by p_i, are calculated similarly to the numerical method employed in this paper as:

$$\frac{dk_{eff}}{dp_i} = \frac{\Delta k_{eff}}{2 \bullet (\Delta p_i)} = \frac{k^+_{eff} - k^-_{eff}}{2 \bullet (p^+_i - p^-_i)} \tag{30}$$

where k_{eff} is the effective multiplication factor from MCNP6 considering the $+\sigma$ and $-\sigma$ perturbations in the resonance parameters.

This approach does not need the multigroup covariance matrices developed in this paper and gets $\left(\sigma_{k_{eff}}\right)^2$ directly from Eqs, (26) through (30) and the resonance parameters covariance matrix given in Table 2. Eq. (30) treats the direct and indirect effects in a straightforward fashion. When a specific ^{238}U resonance parameter is altered, the associated cross sections are altered (Direct effect), which by its turn changes the neutron fluxes in the whole neutron energy domain and consequently all possible reaction rates of all nuclides that constitute the IPEN/MB-01 core (Indirect effect). Due to these features the first approach will be referred to as reference to verify the precision of all other approaches to get the IPEN/MB-01 k_{eff} uncertainties.

The second approach employs the multigroup covariance matrix methods developed in this paper to get the k_{eff} uncertainty. In this case $\left(\sigma_{k_{eff}}\right)^2$ is obtained from Eq. (9) as:

$$\left(\sigma_{k_{eff}}\right)^2 = \sum_g \sum_{g'} \frac{\partial k_{eff}}{\partial \sigma^\gamma_g} \Theta^\gamma_{g,g'} \frac{\partial k_{eff}}{\partial \sigma^\gamma_{g'}} + \sum_g \sum_{g'} \frac{\partial k_{eff}}{\partial \sigma^s_g} \Theta^s_{g,g'} \frac{\partial k_{eff}}{\partial \sigma^s_g} \tag{31}$$

Let equation (31) be written in terms of variances like equation (26) as:

$$\left(\sigma_{k_{eff}}\right)^2 = V^{11,11}_{k_{eff}} + V^{15,15}_{k_{eff}} + V^{11,15}_{k_{eff}} \tag{32}$$

where:

$$V^{11,11}_{k_{eff}} = \frac{\partial k_{eff}}{\partial \sigma^\gamma_{11}} \Theta^\gamma_{11,11} \frac{\partial k_{eff}}{\partial \sigma^\gamma_{11}} + \frac{\partial k_{eff}}{\partial \sigma^s_{11}} \Theta^s_{11,11} \frac{\partial k_{eff}}{\partial \sigma^s_{11}} \tag{33}$$

$$V^{15,15}_{k_{eff}} = \frac{\partial k_{eff}}{\partial \sigma^\gamma_{15}} \Theta^\gamma_{15,15} \frac{\partial k_{eff}}{\partial \sigma^\gamma_{15}} + \frac{\partial k_{eff}}{\partial \sigma^s_{15}} \Theta^s_{15,15} \frac{\partial k_{eff}}{\partial \sigma^s_{15}} \tag{34}$$

Table 14

k_{eff} and its derivative relative to Γ_n e Γ_γ – resonance "1″ and resonance "2".

Resonance	$k_{eff}\Gamma_n + \sigma_{\Gamma_n}$ (*)	$k_{eff}\Gamma_n - \sigma_{\Gamma_n}$	$k_{eff}\Gamma_\gamma + \sigma_{\Gamma_\gamma}$ (*)	$k_{eff}\Gamma_\gamma - \sigma_{\Gamma_\gamma}$	$\frac{dk_{eff}}{d\Gamma_n}$(eV^{-1})	$\frac{dk_{eff}}{d\Gamma_\gamma}$ (eV^{-1})
"1″	0.998099	0.998931	0.998091	0.998947	−27.8633	−1.8609
"2″	0.998351	0.998683	0.998335	0.998709	−1.6179	−0.8162

(*) Here σ_{Γ_n} and σ_{Γ_γ} means the perturbations (1.0%) in the corresponding resonance parameter (either Γ_n or Γ_γ).

$$V_{k_{eff}}^{11,15} = 2 \bullet \frac{\partial k_{eff}}{\partial \sigma_{11}^{\gamma}} \Theta_{11,15}^{\gamma} \frac{\partial k_{eff}}{\partial \sigma_{15}^{\gamma}} + 2 \bullet \frac{\partial k_{eff}}{\partial \sigma_{11}^{s}} \Theta_{11,15}^{s} \frac{\partial k_{eff}}{\partial \sigma_{15}^{s}} \quad (35)$$

The partial variances ($V_{k_{eff}}^{11}$, $V_{k_{eff}}^{11,11}$) and so on although they have different approaches for its determination, they refer to the same quantity. In this way, the comparison between both approaches can be made term a term.

The indirect effect due to the perturbation of the neutron flux mentioned in the first approach is taken into consideration here only in an approximated way. The developments made in Section 3 to derive the covariance matrix neglects the contributions of the nuclides other than ^{238}U. The only indirect effect taken into consideration are those arising from ^{238}U resonances in the specific group g where this resonance occurs. There is no coupling among groups. However, a perturbation in a resonance parameter of a resonance in a generic group g changes the neutron fluxes and the reaction rates at energies below this group. Therefore, there are couplings among neutron energy groups. The only coupling found relevant in the adopted model for the k_{eff} uncertainty analyses of the IPEN/MB-01 reactor is from group15 to group (11). $\Theta_{11,15}^{\gamma}$ and $\Theta_{11,15}^{s}$ in equation (35) have to be redefined by adding the coupling term defined as:

$$coupling term = 2 \bullet \frac{d\sigma_{11}^{k}}{d\Gamma_{\gamma}^{2}} < \Gamma_{\gamma}^{2}, \Gamma_{\gamma}^{2} > \frac{d\sigma_{15}^{k}}{d\Gamma_{\gamma}^{2}} + 2 \bullet \frac{d\sigma_{11}^{k}}{d\Gamma_{n}^{2}} < \Gamma_{n}^{2}, \Gamma_{n}^{2} > \frac{d\sigma_{15}^{k}}{d\Gamma_{n}^{2}} \quad (36)$$

where k stands for γ or s. The coupling term was calculated employing the 3rd methodology (ROLAIDS) similarly to the other terms of Eq. (25).

The set of equations (32) through (35) needs the derivative of k_{eff} to the group cross sections. These derivatives cannot be obtained directly from the numerical approach employed in Sections 3. The procedure adopted here to obtain these derivatives is to write $\frac{dk_{eff}}{d\Gamma_{\gamma}}$ and $\frac{dk_{eff}}{d\Gamma_{n}}$ from Eq. (30) approximately as:

$$\frac{dk_{eff}}{d\Gamma_{\gamma}^{1}} \approx \frac{\partial k_{eff}}{\partial \sigma_{11}^{\gamma}} \bullet \frac{\partial \sigma_{11}^{\gamma}}{\partial \Gamma_{\gamma}^{1}} + \frac{\partial k_{eff}}{\partial \sigma_{11}^{s}} \bullet \frac{\partial \sigma_{11}^{s}}{\partial \Gamma_{\gamma}^{1}} \quad (37)$$

$$\frac{dk_{eff}}{d\Gamma_{n}^{1}} \approx \frac{\partial k_{eff}}{\partial \sigma_{11}^{\gamma}} \bullet \frac{\partial \sigma_{11}^{\gamma}}{\partial \Gamma_{n}^{1}} + \frac{\partial k_{eff}}{\partial \sigma_{11}^{s}} \bullet \frac{\partial \sigma_{11}^{s}}{\partial \Gamma_{n}^{1}} \quad (38)$$

for group (11), and

$$\frac{dk_{eff}}{d\Gamma_{\gamma}^{2}} \approx \frac{\partial k_{eff}}{\partial \sigma_{15}^{\gamma}} \bullet \frac{\partial \sigma_{15}^{\gamma}}{\partial \Gamma_{\gamma}^{2}} + \frac{\partial k_{eff}}{\partial \sigma_{15}^{s}} \bullet \frac{\partial \sigma_{15}^{s}}{\partial \Gamma_{\gamma}^{2}} + \frac{\partial k_{eff}}{\partial \sigma_{11}^{\gamma}} \bullet \frac{\partial \sigma_{11}^{\gamma}}{\partial \Gamma_{\gamma}^{2}} + \frac{d\partial k_{eff}}{\partial \sigma_{11}^{s}} \bullet \frac{\partial \sigma_{11}^{s}}{\partial \Gamma_{\gamma}^{2}} \quad (39)$$

$$\frac{dk_{eff}}{d\Gamma_{n}^{2}} \approx \frac{\partial k_{eff}}{\partial \sigma_{15}^{\gamma}} \bullet \frac{\partial \sigma_{15}^{\gamma}}{\partial \Gamma_{n}^{2}} + \frac{\partial k_{eff}}{\partial \sigma_{15}^{s}} \bullet \frac{\partial \sigma_{15}^{s}}{\partial \Gamma_{n}^{2}} + \frac{\partial k_{eff}}{\partial \sigma_{11}^{\gamma}} \bullet \frac{\partial \sigma_{11}^{\gamma}}{\partial \Gamma_{n}^{2}} + \frac{d\partial k_{eff}}{\partial \sigma_{11}^{s}} \bullet \frac{\partial \sigma_{11}^{s}}{\partial \Gamma_{n}^{2}} \quad (40)$$

for group (15). The word "approximately" means that the contributions of the nuclides other than ^{238}U in Eqs (37) through (40) are neglected. The only coupling taken into consideration is from group15 to group (11). The last two terms of Eq's (39) and (40) accounts for this coupling. The unknowns in this set of equations are the derivatives of k_{eff} to the group cross sections in each group. The derivatives of k_{eff} and the group cross sections to the resonance parameters are given, respectively, in Tables 15 and 5. Consequently, the set of equation (37) through (40) can be solved in a straightforward fashion.

4.7. Numerical results for the uncertainty analyses

Starting from the first approach Table 14 shows k_{eff} calculated by MCNP6 considering the $+\sigma$ and $-\sigma$ perturbations (1.0 %) in the resonance parameters and the derivative of k_{eff} relative to either Γ_n or Γ_γ from Eq. (30).

Table 14 shows that the k_{eff} derivatives independently of the resonance and the resonance parameter considered are always negative. Consequently, the product between any two k_{eff} derivatives in Eqs. (26) through (28) is always positive and the sign of each term of these equations will depend if Γ_n and Γ_γ are correlated or anti-correlated. Table 2 shows that Γ_n and Γ_γ are anti-correlated only for resonance "2″. In this way, considering the correlation between resonance Γ_n and Γ_γ for the same resonance, the k_{eff} uncertainty increases for resonance "1" and decreases for resonance "2".

The effect of the correlation between resonances is more complicated due to the relative contribution of the terms of Eq. (29). Table 15 shows the contributions of each resonance and that of the correlation between them in the determination of the k_{eff} uncertainty. This table shows that the contribution of the correlation between resonances is negative, and due to that the total k_{eff} uncertainty decreases relatively to the case of neglecting this correlation. Also, it can be noted that the k_{eff} total uncertainty is even lower than that of the resonance "1″ contribution. These properties of the of the resonance parameter covariance matrix for the ^{238}U resonances under consideration here are of fundamental importance for the determination and the interpretation of the k_{eff} uncertainty of the IPEN/MB-01 reactor.

The second approach employed the multigroup covariance matrix shown in Table 16. There are four distinct sets: namely MCNP, NJOY, Direct Effect, and Infinite Dilution. The coupled model modifies only the MCNP set and redefines $\Theta_{11,15}^{\gamma}$ and $\Theta_{11,15}^{s}$ by adding the coupling term given by Eq. (36) only. The uncoupled model does not consider Eq. (36). The MCNP values are from Table 13 but the coupling term given by Eq. (36) was from ROLAIDS; the deterministic method. The NJOY values were generated employing the flowchart shown in Fig. 2 and the average weighting flux of all 10 zones from ROLAIDS. The direct approach values were generated by MCNP6. The procedure is like the one employed in Section 4.4.3. Here, MCNP6 runs were made for the unperturbed cases and the reaction rate tallies were requested employing the perturbed cross sections ($+\sigma$ and $-\sigma$). The derivative of the cross sections to the resonance were performed employing Eqs. (19) and (20). The Infinite Dilution values were calculated considering the weighting flux equal to C/E for the determination of $\frac{d\sigma^{kg}}{dp_i}$ as in Table 5 of Section 0.4.3. The elements of the multigroup covariance matrix for the Direct Effect and the Infinite Dilution cases were calculated employing Eqs. (23) through (25).

The k_{eff} derivatives to the group cross sections from the solution of the set of equations (37) through (40) are shown in Table 17.

The derivatives of k_{eff} relative to the group cross section is in accordance with the physics of thermal reactors. This derivative is negative for the (n,γ) events and positive for scattering events.

The IPEN/MB-01 k_{eff} uncertainty analyses are shown in Tables 19 and 20. The uncertainty analyses shown in Tables 19 and 20 employs the k_{eff} derivatives to the group cross sections from MCNP6 coupled case showing in Table 17. The reason for that was to compare the k_{eff} uncertainty analyses arising from different methos in the same basis. The

Table 15
k_{eff} Uncertainty and the impact of the resonance contribution.

$V_{k_{eff}}^{11}$	$V_{k_{eff}}^{22}$	$V_{k_{eff}}^{11} + V_{k_{eff}}^{22}$	$V_{k_{eff}}^{12}$	TOTAL
3.54309E-06	1.75997E-06	5.30306E-06	−1.89822E-06	3.40483E-06
k_{eff} Uncertainty Contribution (pcm)	k_{eff} Uncertainty Contribution (pcm)	k_{eff} Uncertainty Contribution (pcm)	–	k_{eff} Total Uncertainty (pcm)
188	133	231	–	185

Table 16
The elements of the multigroup covariance matrix at 293 K (barn^2).

Element	Reaction	MCNP	NJOY	Direct Effect	Infinite Dilution
Element	Reaction	MCNP	NJOY	Direct Effect	Infinite Dilution
$\Theta^k_{11,11}$					
	Capture	0.2015	0.5956	0.8046	1.0875E + 02
	Elastic	0.0083	0.0217	0.0165	2.8788E + 00
$\Theta^k_{15,15}$					
	Capture	0.3230	0.4324	0.5699	2.8429E + 02
	Elastic	3.8793	3.0943	5.0461	3.1949E + 03
$\Theta^k_{11,15}$					
Uncoupled	Capture	−0.1864	−0.1303	−0.2785	7.2830E + 01
	Elastic	0.1172	−0.1572	0.1812	1.9844E + 01
$\Theta^k_{11,15}$					
Coupled	Capture	−0.0805	-	-	-
	Elastic	0.1172	-	-	-
$\Theta^k_{11,11}$					
	Capture	0.2015	0.5956	0.8046	1.0875E + 02
	Elastic	0.0083	0.0217	0.0165	2.8788E + 00
$\Theta^k_{15,15}$					
	Capture	0.3230	0.4324	0.5699	2.8429E + 02
	Elastic	3.8793	3.0943	5.0461	3.1949E + 03
$\Theta^k_{11,15}$					
Uncoupled	Capture	−0.1864	−0.1303	−0.2785	7.2830E + 01
	Elastic	0.1172	−0.1572	0.1812	1.9844E + 01
$\Theta^k_{11,15}$					
Coupled	Capture	−0.0805	-	-	-
	Elastic	0.1172	-	-	-

Table 17
k_{eff} derivatives to the group cross sections (barn/eV).

Group (11)		**Group (15) Coupled**		**Group (15) Uncoupled**	
$\frac{\partial k_{eff}}{\partial \sigma^{\gamma}_{11}}$	$\frac{\partial k_{eff}}{\partial \sigma^{s}_{11}}$	$\frac{\partial k_{eff}}{\partial \sigma^{\gamma}_{15}}$	$\frac{\partial k_{eff}}{\partial \sigma^{s}_{15}}$	$\frac{\partial k_{eff}}{\partial \sigma^{\gamma}_{15}}$	$\frac{\partial k_{eff}}{\partial \sigma^{s}_{15}}$
−4.2674E-03	1.1949E-04	−2.1053E-03	5.1188E-05	−2.1760E-03	8.2575E-05

Table 18
Individual and total k_{eff} variances for each set. (dimensionless).

Reference				
$V^{11}_{k_{eff}}$	$V^{22}_{k_{eff}}$	$V^{11}_{k_{eff}} + V^{22}_{k_{eff}}$	$V^{12}_{k_{eff}}$	$V^{11}_{k_{eff}} + V^{22}_{k_{eff}} + V^{12}_{k_{eff}}$
3.54309E-06	1.75997E-06	5.30306E-06	−1.89822E-06	3.40483E-06
$V^{11.11}_{k_{eff}}$	$V^{15.15}_{k_{eff}}$	$V^{11.11}_{k_{eff}} + V^{15.15}_{k_{eff}}$	$V^{11.15}_{k_{eff}}$	$V^{11.11}_{k_{eff}} + V^{15.15}_{k_{eff}} + V^{11.15}_{k_{eff}}$
MCNP6 Uncoupled				
3.66983E-06	1.55612E-06	5.22595E-06	−3.45979E-06	1.76616E-06
MCNP6 Coupled				
3.66983E-06	1.44201E-06	5.11184E-06	−1.44660E-06	3.66596E-06
NJOY				
1.0247E-05	1.8916E-06	1.2139E-05	−2.25895E-06	9.8798E-06
Direct Effect				
1.38433E-05	2.4948E-06	1.6338E-05	−4.82634E-06	1.1512E-05
Infinite Dilution				
1.8709E-03	1.2452E-03	3.1161E-03	1.26249E-03	4.3785E-03

quantity that changes from method to method is the multigroup covariance matrix and the quality of this matrix can be analyzed in a straightforward fashion. Particularly the indirect effect contribution can be noted by comparing to the k_{eff} uncertainty from these methods either to the reference case or to the coupled MCNP6 case of Table 17.

Table 18 shows the individual variances for each set of multigroup covariance matrix. The reference case is also shown for easy comparison. This Table shows that the coupled case among all cases has an excellent agreement to the reference case for all individual variances. The uncoupled case reproduces well $V^{11,11}_{k_{eff}}$ and $V^{11,11}_{k_{eff}} + V^{12,12}_{k_{eff}}$, but it does not show the nearly cancellation of $V^{22}_{k_{eff}}$ and $V^{12}_{k_{eff}}$ observed in the reference and in the coupled cases. Surprisingly, NJOY has a good agreement for $V^{22}_{k_{eff}}$ but this agreement is not observed for the other individual variances. Particularly, its total variance is well overpredicted. This finding demonstrates that the coupling among resonance in different groups may have an important bearing in the determination of the k_{eff} uncertainty. The effect of neglecting the Indirect Effect can be noted by comparing the Direct Effect results to those of the MCNP6 coupled case. With exception to $V^{12}_{k_{eff}}$, the Direct Effect systematically overpredicts its results for all other individual variance. $V^{12}_{k_{eff}}$ is negative and in this case the Direct Effect underestimate this variance.

Table 19 shows the k_{eff} uncertainty analyses for each set of multigroup covariance matrix. The reference k_{eff} uncertainties are also repeated in this table for easy comparison. Here, the comparison follows closely that already discussed for the variances. The coupled model shows the best performance. Contrary to that, the uncoupled model does not show the same performance and underestimates the total k_{eff} uncertainty. All other models overpredict the total k_{eff} uncertainty in a large extent. NJOY, also here, has only a good agreement to $\sqrt{V^{22}_{k_{eff}}}$. Its total uncertainty shows a large discrepancy to the reference value. The Direct Effect comparison to the coupled model shows the impact of neglecting the indirect effect. The indirect effect may account for nearly 44% of the total k_{eff} uncertainty. The Infinite Dilution values are shown here just to illustrate the importance of considering the self-shielding effects in the multigroup covariance matrix.

Table 20 shows the relative contribution of the capture and elastic cross sections to the total k_{eff} uncertainty. This table shows, as expected, that the elastic has very little bearing on the total k_{eff} uncertainty.

5. Conclusions

Numerical approaches have been successfully developed to propagate the resonance parameter uncertainties to the multigroup covariance matrices and, either directly from the resonance parameters or indirectly from multigroup covariance matrices, to the k_{eff} of a critical configuration of the IPEN/MB-01 reactor. The approaches were developed for the groups containing the two most important ^{238}U resonances. The k_{eff} uncertainty analyses performed in the critical configuration of the IPEN/MB-01 reactor reveal that the self-shielding effects as well as the indirect effect in the multigroup covariance matrix are severe and must be taken into consideration in the uncertainty analyses of integral responses of nuclear reactors. The differences for considering and not considering the indirect effects are observed in the magnitude of the components of the covariance matrix, in their sign as well and in the k_{eff} uncertainty analyses. Particularly in this last item the analyses performed to the critical configuration of the IPEN/MB-01 reveal that the indirect effect is responsible for around 45% of the total k_{eff} uncertainty. The comparison between ROLAIDS and MCNP6 results for $\frac{d\sigma^{kg}}{dp_i}$ come into a good agreement and supports the developments performed and the conclusions reached in this work. There are two major differences between the NJOY approach and those of this work. First, the ERRORR module of NJOY employs the Breit-Wigner formalism always at 0 K to calculate the derivative of the cross sections to the resonance parameters and second ERRORR takes into account only the direct effect on the multigroup covariance matrix. Particularly, the second difference is by

Table 19
The IPEN/MB-01 k_{eff} uncertainty analyses.

Reference			
$\sqrt{V_{k_{eff}}^{11}}$(pcm)	$\sqrt{V_{k_{eff}}^{22}}$) (pcm)	$\sqrt{V_{k_{eff}}^{11}+V_{k_{eff}}^{22}}$(pcm)	$\sqrt{V_{k_{eff}}^{11}+V_{k_{eff}}^{22}+V_{k_{eff}}^{12}}$(pcm)
188	133	230	185
$\sqrt{V_{k_{eff}}^{11.11}}$(pcm)	$\sqrt{V_{k_{eff}}^{15.15}}$) (pcm)	$\sqrt{V_{k_{eff}}^{11.11}+V_{k_{eff}}^{15.15}}$(pcm)	$\sqrt{V_{k_{eff}}^{11.11}+V_{k_{eff}}^{15.15}+V_{k_{eff}}^{11.15}}$(pcm)
MCNP6 Uncoupled			
192	125	229	133
MCNP6 Coupled			
192	120	226	191
NJOY			
320	139	348	315
Direct Effect			
372	159	405	339
Infinite Dilution			
4325	3529	5582	6617

Table 20
The Partial contributions of the capture and elastic cross section to the k_{eff} uncertainty (%).

Reaction	MCNP6 Coupled	MCNP6 Uncoupled	NJOY	Direct Effect
Capture	99.86	97.96	99.96	99.94
Elastic	0.14	2.04	0.04	0.06

far the most important and it will impose severe restrictions to the multigroup covariance matrices generated by the ERROR module of NJOY. Finally, the ENDF FILE 33 can not be interpreted as application independent. Its content must be corrected due to the resonance self-shielding effects and also to the indirect effects and methods must be developed to take this effect into consideration mainly for thermal reactor applications.

Declaration of Competing Interest

The authors declare that they have no known competing financial interests or personal relationships that could have appeared to influence the work reported in this paper.

Data availability

Data will be made available on request.

References

Arbanas, G., Sobes, V., Holcomb, A., Ducru, P., Pigni, M., Wiarda, D., Plompen, A., Hambsch, F.-J., Schillebeeckx, P., Mondelaers, W., Heyse, J., Kopecky, S., Siegler, P., Oberstedt, S., 2017. Generalized Reich-Moore R-matrix approximation. EPJ Web Conf. 146, 12006.

J Barhen, W Rothenstein, E Taviv Barhen, J., et al., 1978. The HAMMER Code System. Technion- Israel Institute of Technology, Haifa Israel. EPRI-NP-565 TRN: Tab9-002832. doi: 10.2172/6516278.

Bell, G.I., Glasstone, S., 1979. Nuclear Reactor Theory. Robert E. Krieger Publishing Company, Huntington, New York, USA.

Boyarinov, V.F., Grol, A.V., Fomichenko, P.A., Ternovykh, M.Y., 2017. Improvement of modeling HTGR Neutron physics by Uncertainty Analysis with the use of cross-section covariance information. J. Phys.: Conf. Ser. 781, 012032.

Breit, G., Wigner, E., 1936. Capture of Slow Neutrons. Phys. Rev. 49 (7), 519–531.

Brown, D.A., et al., 2018. ENDF/B-VIII.0: The 8th Major Release of the Nuclear Reaction Data Library with CIELO-project Cross Sections, New Standards and Thermal Scattering Data. Nucl. Data Sheets 148, 1–142.

Brown, F.B. et al., J.L., 2016. MCNP-WHISPER Methodology for Nuclear Criticality Safety Validation. LA-UR-16-23757.

Chadwick, M., et al., 2006. ENDF/B- VII.0: Next Generation Evaluated Nuclear Data Library for Nuclear Science and Technology. Nucl. Data Sheets 107 (12), 2931–3060.

Chiba, G.O., Tsuji, Amsashi, Narabayashi, Tadashi, 2014. Resonance Self-Shielding Effect in Uncertainty Quantification of Fission Reactor Neutronics Parameters. Nucl. Eng. and Technol. 46 (3), 281–290.

Chiba, G., 2006. Resonance Self-Shielding Effect in Covariance Processing. Workshop Proc. for Perspectives on Nuclear Data for the Next Decade. P(ND)2, OECD/NEA No.6121, 227-231.

Chiba, G., 2007. ERRORJ: A Code to Process Neutron-Nuclide Reaction Cross Section Covariance, Version 2.3. Japan Atomic Energy Agency, JAEA-Data/Code 2007-007.

Cullen D.E., 2010. PREPRO 2010. Tech. Rep. IAEA-NDS-39, International Atomic Energy Agency.

Dos Santos, A., 1984. A Differential approach to Sensitivity Analysis of Transmutation Analysis Problems. University of Wisconsin, Madison. Ph. D. Thesis.

Dos Santos, A., et al., 2004. LEU-COMP-THERM-077: Critical Loading Configurations of the IPEN/MB-01 Reactor. In: Briggs, J.B. (Ed.), International Handbook of Evaluated Criticality Safety Benchmark Experiments. NEA/NSC/DOC (95)03/I, Paris.

Dos Santos, A., et al., 2005. LEU-COMP-THERM-082: Critical loading Configurations of the IPEN/MB-01 Reactor Considering Low Enriched Fuel and Burnable Poison Rods. In: Briggs, J.B. (Ed.), International Handbook of Evaluated Criticality Safety Benchmark Experiments. NEA/NSC/DOC (95)03/I, Paris.

Dos Santos, A., et al., 2000. Criticality Analyses Based on The Coupled NJOY/AMPX-II/TORT Systems. ANS International Topical Meeting on Advances in Reactor Physics and Mathematics and Computation into the Next Millennium, May 7-12, 2000, Pittsburgh, PA, USA.

Dos Santos, A., et al., 2018. IPEN(MB01)-LWR-RESR-017: The Inversion Point of the Isothermal Reactivity Coefficient of the IPEN/MB-01 Reactor. In: Briggs, J. Blair (Ed.), in: International Handbook of Evaluated Reactor Physics Benchmark Experiments. Paris: Nuclear Energy Agency, Paris (March Edition 2018).

Garber, D., 1975. ENDF/B Summary Documentation. BNL-17541, 2nd Edition.

Green, N.M., et al., 1976. AMPX-II A Modular Code System for Generation Coupled Multigroup Neutron-Gamma Libraries from ENDF/B. ORNL-TM-3706.

Hiruta, H., Palmiotti, G., Salvatores, M., Arcilla, R., Obložinský, P., McKnight, R.D., 2008. Few Group Collapsing of Covariance Matrix Data Based on a Conservation Principle. Nucl. Data Sheets 109 (12), 2801–2806.

Hursin, M., Pelloni, S., Vasiliev, A., Ferroukhi, H., 2020. Treatment of the implicit effect in Shark-X. Ann. Nucl. Energy 138, 107178.

Kawano, T., Shibata, K., 1997. Covariance Evaluation System. JAERI-Data/Code–97-037 [in Japanese].

Larson, N.M., 2008. Updated Users's Guide for SAMMY: Multi-level R-Matrix Fits to Neutron Data Using Bayeś Equations. ORNL/TM-9179/R8. DP0902090; DPDP097; ENDF-364/R2; TRN: US0807450. http://doi.org/10.2172/941054.

Leal, L., de Saint Jean, C., 2018. Resonance parameter covariance representation: FILE32 versus FILE33. EPJ Nucl. Sci. Technol. 4, 17.

Leal, L.C., et al., 2005. A New Approach for Nuclear Data Covariance and Sensitivity Generation. International Conference on Nuclear Data for Science and Technology, New York: American Institute of Physics, pp. 338-341.

MacFarlane, R.E., 2019. The NJOY Nuclear Data Processing System, Version 2016. LA-UR-17-20093, December 19, 2016. Updated for NJOY2016.53 November 7, 2019.

NRC, 2012. Acceptance Criteria for Emergency Core Cooling Systems for Light-Water Nuclear Power Reactors. US Code of Federal Regulations, Title 10, Part 50, Section, 46. Nuclear Regulatory Commission, Rockville, MD. Oak Ridge National Laboratory, TN (USA). ORNL/TM-7221.

Otuka, N., Zukeran, A., Takano, H., Chiba, G.o., Ishikawa, M., 2008. Covariance Analyses of Self-Shielding Factor and Its Temperature Gradient for Uranium-238 Neutron Capture Reaction. Nucl. Sci. Technol. 45 (3), 195–210.

Peelle, R.W., 1982. Uncertainty in the Nuclear Data Used for Reactor Calculations. In: Lewins, J., Becker, M. (Eds.), Advances in Nuclear Science and Technology. Springer US, Boston, MA, pp. 11–84.

Perey, F.G., 1977. The Data Covariance FILEs for ENDF/B-V. Oak Ridge National Laboratory, TN (USA). ORNL/TM-5938.

Perey, F.G., 1978. Expectations For ENDF/B-V Covariance FILEs: Coverage, Strength, and Limitations. Oak Ridge National Laboratory, TN (USA) CONF-780858-6/TRN, 79–007362.

Plompen, A.J.M., et al., 2020. The joint evaluated fission and fusion nuclear data library, JEFF-3.3. Eur. Phys. J. A 56, 181. https://doi.org/10.1140/epja/s10050-020-00141-9.

Rochman, D., Leray, O., Hursin, M., Ferroukhi, H., Vasiliev, A., Aures, A., Bostelmann, F., Zwermann, W., Cabellos, O., Diez, C.J., Dyrda, J., Garcia-Herranz, N., Castro, E., van der Marck, S., Sjöstrand, H., Hernandez, A., Fleming, M., Sublet, J.-C., Fiorito, L., 2017. Nuclear Data Uncertainties for Typical LWR Fuel Assemblies and a Simple Reactor Core. Nucl. Data Sheets 139, 1–76.

Rose, P.F., 1991. ENDF-201: ENDF/B-VI Summary Documentation. BNL-NCS-17541, 4th ed. Brookhaven National Laboratory.

Shibata, K., et al., 2002. Japanese Evaluated Nuclear Data Library, Version 3, Revision-3: JENDL-3.3. Journal of Nucl. Sci. and Technol., 39 (11), 1125–1136.

Shibata, K., Iwamoto, O., Nakagawa, T., Iwamoto, N., Ichihara, A., Kunieda, S., Chiba, S., Furutaka, K., Otuka, N., Ohsawa, T., Murata, T., Matsunobu, H., Zukeran, A., Kamada, S.o., Katakura, J.-I., 2011. JENDL-4.0: A New Library for Nuclear Science and Engineering. J. Nucl. Sci. Technol. 48 (1), 1–30.

Smith, D.L., 1981. Covariance matrices and applications to the field of nuclear data. Argonne National Lab. IL (USA), ANL/NDM-62.

Smith, J. D., 1980. Processing ENDF/B-V uncertainty data into multigroup covariance matrices. Oak Ridge National Laboratory, TN (USA). ORNL/TM-7221; ENDF-295 TRN: 80-013510.

Sobes, V., Holcomb, A., Marshall, B.J., Greene, T., Wiarda, D., Wieselquist, W., 2021a. Augmented ENDF/B-VIII.0 covariance library for SCALE 6.3. Ann. Nucl. Energy 160, 108353.

Sobes, V., de Saint Jean, C., Rochman, D., Cabellos, O., Holcomb, A., Bauge, E., Capote, R., Trkov, A., Fleming, M., 2021b. WPEC Subgroup 44 computational Inter-comparison exercise on correlations in nuclear data libraries. Ann. Nucl. Energy 164, 108605.

Takeda, T., Foad, B., 2013. Development of Calculation Method of Sensitivities for Light Water Reactors. Nucl. Eng. Technol. 45 (6), 753–758.

Trkov, A., Brown, D. A., 2018. ENDF-6 Formats Manual: Data Formats and Procedures for the Evaluated Nuclear Data Files. Report BNL-203218-2018-INRE https://doi: 10.2172/1425114.

Vanhanen, R., 2015. Computing More Consistent Multigroup Nuclear Data Covariances. Nucl. Sci. Eng. 181 (1), 60–71. https://doi.org/10.13182/NSE14-105.

Velleman, D.J., 2005. The Generalized Simpson's Rule. The American Mathematical Monthly 112 (4), 342–350. https://doi-org.ez67.periodicos.capes.gov.br/10.2307/30037470.

Wieselquist, W.A., Lefebvre, R.A. (Eds.), 2023. SCALE 6.3.1 User Manual, ORNL/TM-SCALE-6.3.1, UT-Battelle. LLC, Oak Ridge National Laboratory, Oak Ridge, TN.

Werner, C.J., et al., 2018. MCNP6. 2 Release Notes. Los Alamos National Laboratory: report LA-UR-18-20808. doi: 10.2172/1419730.

Wiarda, D., et al., 2008. Recent Advances with the AMPX Covariance Processing Capabilities in PUFF-IV. Nucl. Data Sheets 109 (12), 2791-2795. https://doi-org.ez67.periodicos.capes.gov.br/10.1016/j.nds.2008.11.011.

Yu, J., et al., 2018. Implicit Resonance Self-Shielding Effect of Multi-Group Covariance in RXSP Code. Transactions of the Korean Nuclear Society Spring Meeting.

Zhang, Q., Wu, H., Cao, L., Zheng, Y., 2015. An improved resonance self-shielding calculation method based on equivalence theory. Nucl. Sci. Eng. 179 (3), 233–252.

Zwermann, W., et al., 2011. Uncertainty analyses with nuclear covariance data in reactor core calculations. J. Korean Phys. Soc. 59 (2), 1256–1259. https://doi.org/10.3938/jkps.59.1256.